Core hole polarization in resonant photoemission

Core hole polarization in resonant photoemission

Gerrit van der Laan† and B T Thole‡

† Daresbury Laboratory, Warrington WA4 4AD, UK
‡ Material Science Center, University of Groningen, 9747 AG Groningen, The Netherlands

Abstract. A theory is presented for core hole polarization probed by spin polarization and magnetic dichroism in resonant photoemission. The resonant photoemission is considered as a two-step process, starting with an excitation from a core level to the valence shell, after which the core hole decays into two shallower core holes while an electron is emitted. The two core holes form well defined states which can be selected by the energy of the emitted electron. The non-spherical core hole and the selected final state cause a specific angle and spin distribution of the emitted electron. The experiment is characterized by the magnetic and non-magnetic moments being measured, the polarization and direction of the light and the spin and angular distribution of the emitted electron. The intensity is a sum over ground state expectation values of tensor operators multiplied by the probability of creating a polarized core hole using polarized light, multiplied by the probability for decay of such a core hole into the final state. Using diagrammatic methods we derive general expressions for the angle and spin dependent intensity in various regimes of Coulomb and spin–orbit interaction, LS, LSJ and jjJ coupling. This core polarization analysis generalizes the use of sum rules in x-ray absorption spectroscopy where the integrated peak intensities give ground state expectation values of operators such as the spin and orbital moments. The photoemission decay makes it possible to measure new linear combinations of operators. The general formula for second-order processes shows that in the presence of core–valence interactions the two-step model may break down due to interference terms between intermediate states separated by more than their lifetime width. We present tables for the resonant p core hole decays in 3d transition metals. The $2p_{3/2}3p3p$ decay in ferromagnetic nickel is calculated using Hartree–Fock values for the radial matrix elements and phase factors. Recent measurements show an effect which is smaller in the ${}^3P$ final state but stronger in the ${}^1D$, ${}^1S$ peak. Spin polarization is due to odd moments of the core hole. We discuss and plot angular distributions and suitable geometries for spin polarized detection.

1. Introduction

Core level photoemission is important for the study of the electronic and magnetic properties of 3d transition metal, rare earth and actinide compounds. Due to the electrostatic core–valence interactions the final state configurations of these materials display characteristic features that contain information on the ground state. Recent progress in devices for circularly polarized synchrotron radiation have made it possible to explore also the polarization dependence of the core excitations. Polarized photoemission from core levels is due to the alignment of the valence band orbital and spin moments with the moments of the core hole created. In a series of three papers we have treated the spin polarization and magnetic dichroism in photoemission from core and valence states in localized magnetic systems. In paper I [1] we defined fundamental spectra directly connected to ground state operator expectation values. In paper II [2] we showed that emission from an incompletely filled localized shell obeys sum rules which relate the integrated intensities of e.g. the

magnetic circular dichroism and spin spectrum to the ground state orbital and spin magnetic moment. In paper III [3] the geometry was separated from the physical properties and the angular dependence was shown to exhibit higher magnetic moments. The interference term between the $l-1$ and $l+1$ emission channels allows us to measure the odd magnetic moments with linearly polarized light in a chiral geometry.

Apart from photoemission we can also use x-ray absorption spectroscopy (XAS) to study the magnetic properties in the ground state [4]. In XAS a core electron is excited into a polarized valence state and the dipole selection rules together with the Pauli principle result in a difference in absorption probability for left and right circularly polarized light. We can consider XAS as a method which simply counts the number of core holes produced in the absorption irrespective of their kind. In total electron yield detection each core hole will mainly be filled by autoionization or Auger decay emitting electrons which are then measured. In transmission mode simply all photons absorbed are counted which is supposed to give the same result. There are simple sum rules for the integrated signals in XAS which give the orbital and spin magnetization, the spin–orbit operator $l \cdot s$ and the quadrupole moment of the ground state [5–10]. However, instead of merely counting the emitted electrons we can also detect their direction, spin and energy. Because each type of core hole emits electrons in different directions and with different spin polarization decaying to different final states we can obtain more detailed information on the core hole produced by the absorption step and this gives improved knowledge of the original valence shell polarization.

Resonant photoemission combines absorption and emission. This technique has been widely used to enhance the valence band photoemission by a super-Coster–Kronig decay after photon excitation at a shallow core level absorption edge, such as the 3p edge in 3d transition metals [11–13] or the 4d edge in rare earths [14–17]. At these edges the direct and resonant photoemission are of the same order of magnitude, resulting in complicated interference effects [18–21]. At deeper core levels the ratio of the cross-section for x-ray absorption to that of direct photoemission is much larger, producing an enhancement by a factor of 10–100. The interference between the two channels is then negligible allowing a much more straightforward analysis. Such a strong photoemission enhancement was found at resonance with the 2p absorption in 3d transition metal compounds [22–29] and the 3d absorption in rare earth materials [30–32]. These studies have helped to clarify the decay mechanisms and the assignment of charge-transfer satellites, e.g. in transition metal oxides [33, 34].

Tjeng *et al* [35] have measured the 2p3d3d decay from the $2p_{3/2}$ absorption edge of ferromagnetic nickel using circularly polarized light. The magnetic circular dichroism confirmed the localized character of the final states in XAS. In that study the angular dependence of the emission was not taken into account. The magnetic dichroism in the photoemission decay is then simply determined by the difference in the amount of holes created with left and right circularly polarized light in the XAS process. The decay rate does not depend on the polarization of the valence shell because in the intermediate state it is in a d^{10} configuration, nor on that of the core hole because this polarization does influence the direction of emission but not the integrated photoemission *per hole* created. Therefore, just as in x-ray absorption using total electron yield in this case only the monopole of the core hole was measured.

The decay to final states with one or two *core* holes also gives strong resonance structures [24–27, 36]. Recently, Thole *et al* [37] measured a magnetic circular dichroism signal of 9% in the 2p3p3p decay of ferromagnetic nickel in a geometry where the circular dichroism in the 2p XAS is forbidden, i.e. with the helicity vector of the light perpendicular to the

magnetization direction. The magnetic dichroism in the angle integrated photoemission is then zero; however the magnetic dichroism in the photoemission along a non-collinear direction is not zero but provides a direct probe for the quadrupole moment of the core hole state. This has the effect that with resonant photoemission we can measure combinations of the ground state multipole moments other than those obtained from XAS.

Autoionization and related phenomena, such as two-photon excitation and Auger coincidence spectroscopy, have already been studied extensively in atomic physics [38–55] where the main aim was to perform 'complete experiments' and to use known polarizations of the initial state in order to determine the radial matrix elements and phase shifts of the interfering decay channels [44]. As in the case of non-resonant photoemission in paper III our approach for the solid state is the opposite. We assume that the radial matrix elements and phase factors for photoemission from deep core levels are known, e.g. from atomic Hartree–Fock calculations [56]. We use this complete knowledge of the decay process to study the polarization in the ground state caused by solid state interactions, such as the molecular field (exchange interaction).

In the present paper we will treat resonant photoemission as an absorption step followed by a decay. In the absorption step the ground state polarization and the polarization of the light produce a polarized core hole. The emission step can be considered as a tool to explore this 'core hole polarization'. It is advantageous to study the decay from the deep-core-hole state into a shallower-double-core-hole state. In this case there is no direct photoemission and moreover the double-core-hole state is highly localized having a well defined wave function. Decay processes involving open shells, such as core–core–valence and core–valence–valence decays, are more complicated and will not be discussed in this paper. In Ni d^9 however the absorption step produces a p^5d^{10} configuration, so that we may consider d^{10} as the core level to use as a detector of the p core hole polarization.

The simplest example of core hole polarization has already been used to analyse the classic experiments on the 3p3d3d decay of ferromagnetic nickel considering only the spin [57,58]. In the 3p3d3d decay most intensity goes to a ^1G final state, where the two spins are paired. Since the spin is conserved in both the absorption and decay processes, the measurement of the photoelectron spin reveals the spin of the intermediate 3p core hole and therefore of the initial hole in the 3d valence band.

We will consider here excitation from core levels deeper than 3p, which have a large spin–orbit splitting. This gives the possibility of studying spin properties by measuring angular distributions without spin detection. Our approach in terms of a two-step process [59–61] neglects interference effects due to electrostatic core–valence interactions. This will cause deviations from the simple behaviour presented here. On the other hand the deviations contain information on the core–valence interactions which can be used to test the validity of the one-electron model. There is also an obvious third step, *viz.* the transmission of the excited electron to the detector. Since the scattering of the photoelectron in the solid has already been quite successfully treated [62–65] we will not discuss this last step here. However, especially in the case of forward scattering non-negligible effects may be present.

The outline of this paper is as follows. In section 2 we give a simple presentation of core hole polarization and show how extra information about the ground state operator expectation values can be extracted by detecting resonant photoemission instead of total electron yield. The general theory is presented in section 3, where we show how the process can be decomposed into an excitation and a decay step. Results are given for three different types of coupling scheme: LS, LSJ and jjJ. We discuss the validity of this decomposition into two steps and the interference between the continuum channels in section 4. The characteristics of some special final states are discussed in section 5.

The angle dependence and symmetry properties of the experiment including spin detection are given in section 6. In order to enable the use of core hole polarization analysis of experiments we present in sections 6 and 7 tables of the coefficients for creation of a core hole with specific multipole moments and coefficients for the decay into the states LS (or J), in terms of the multipole Coulomb operators and the angle dependent functions including spin polarization. As an application and to practise the use of the tables we analyse the measured Ni 2p3p3p decay data and predict the 2p3p3d and 2p3d3d decays. Conclusions are given in section 8. Appendix A has been added to define coupled tensors and appendix B derives general properties of angle dependent functions, especially concerning parity.

2. Basics

We will introduce here in simple terms the principle of core hole polarization using the example of the $2p_{3/2}$ core hole in a transition metal with holes of $3d_{5/2}$ symmetry. The core level $j' = \frac{3}{2}$ has sublevels $m_{j'}$ which in the initial state are all occupied. The valence level $j = \frac{5}{2}$ has sublevels m_j which are partly occupied. We will use $\langle m_j \rangle$ to indicate the expectation value of the number of holes in each m_j sublevel of the valence level. In second-quantization notation this would be $\langle m_j \rangle = \langle a_{jm_j} a^\dagger_{jm_j} \rangle$.

From spectroscopy we can extract information about the valence shell which may be expressed by giving all the hole occupation numbers. Normally we do not obtain them all but only acquire statistical information. This however is often exactly what we need. This statistics is most properly expressed in *multipole moments* or *state multipoles* [66], formally defined as

$$\langle w^z \rangle = \sum_{m_j} \langle m_j \rangle (-)^{j-m_j} \begin{pmatrix} j & z & j \\ -m_j & 0 & m_j \end{pmatrix} \begin{pmatrix} j & z & j \\ -j & 0 & j \end{pmatrix}^{-1}. \tag{1}$$

Evaluation of the $3j$-symbols results in a simple set of orthogonal operators containing m_j to the power z

$$\langle w^0 \rangle = \sum_{m_j} \langle m_j \rangle = \langle n \rangle \tag{2}$$

$$\langle w^1 \rangle = \sum_{m_j} \langle m_j \rangle \frac{m_j}{j} = \frac{\langle J_z \rangle}{j} \tag{3}$$

$$\langle w^2 \rangle = \sum_{m_j} \langle m_j \rangle \frac{3m_j^2 - j(j+1)}{j(2j-1)} = \frac{\langle 3J_z^2 - J^2 \rangle}{j(2j-1)} \tag{4}$$

$$\langle w^3 \rangle = \sum_{m_j} \langle m_j \rangle \frac{5m_j^3 - m_j[3j(j+1)-1]}{j(j-1)(2j-1)} = \frac{\langle 5J_z^3 - J_z(3J^2-1) \rangle}{j(j-1)(2j-1)} \tag{5}$$

$$\langle w^4 \rangle = \sum_{m_j} \langle m_j \rangle \frac{35m_j^4 - 5m_j^2[6j(j+1)-5] + 3(j-1)j(j+1)(j+2)}{2j(j-1)(2j-1)(2j-3)}$$

$$= \frac{\langle 35J_z^4 - 5J_z^2(6J^2-5) + 3J^2(J^2-2) \rangle}{2j(j-1)(2j-1)(2j-3)} \tag{6}$$

where $J^2 = j(j+1)$.

Before treating the core hole polarization we will first show that in x-ray absorption using polarized radiation we can measure the moments with $z = 0, 1, 2$. The transition

probabilities with left circularly ($q = -\Delta m_j = 1$), Z linearly ($q = -\Delta m_j = 0$) and right circularly ($q = -\Delta m_j = -1$) polarized light are given by the squared $3j$-symbol

$$\begin{pmatrix} j' & 1 & j \\ m_{j'} & q & m_j \end{pmatrix}^2. \tag{7}$$

The intensities for the allowed dipole transitions from $j' = \frac{3}{2}$ to $j = \frac{5}{2}$ are given in figure 1. We are interested in the intensities I^a which are linear combinations of the intensities with different q. The isotropic intensity ($a = 0$) is the sum for $q = +1, 0, -1$. The MCD ($a = 1$) is the $q = 1$ minus $q = -1$ intensity and the linear dichroism ($a = 2$) is the sum of the $q = +1$ and $q = -1$ intensities minus twice the $q = 0$ intensity. We thus obtain for the intensities from each of the $m_{j'}$ sublevels

$$I^0(-\tfrac{3}{2}) = \tfrac{10}{60}\langle-\tfrac{5}{2}\rangle + \tfrac{4}{60}\langle-\tfrac{3}{2}\rangle + \tfrac{1}{60}\langle-\tfrac{1}{2}\rangle$$
$$I^0(-\tfrac{1}{2}) = \tfrac{6}{60}\langle-\tfrac{3}{2}\rangle + \tfrac{6}{60}\langle-\tfrac{1}{2}\rangle + \tfrac{3}{60}\langle+\tfrac{1}{2}\rangle$$
$$I^0(+\tfrac{1}{2}) = \tfrac{3}{60}\langle-\tfrac{1}{2}\rangle + \tfrac{6}{60}\langle+\tfrac{1}{2}\rangle + \tfrac{6}{60}\langle+\tfrac{3}{2}\rangle$$
$$I^0(+\tfrac{3}{2}) = \tfrac{1}{60}\langle+\tfrac{1}{2}\rangle + \tfrac{4}{60}\langle+\tfrac{3}{2}\rangle + \tfrac{10}{60}\langle+\tfrac{5}{2}\rangle \tag{8}$$
$$I^1(-\tfrac{3}{2}) = -\tfrac{10}{60}\langle-\tfrac{5}{2}\rangle + \tfrac{1}{60}\langle-\tfrac{1}{2}\rangle$$
$$I^1(-\tfrac{1}{2}) = -\tfrac{6}{60}\langle-\tfrac{3}{2}\rangle + \tfrac{3}{60}\langle+\tfrac{1}{2}\rangle$$
$$I^1(+\tfrac{1}{2}) = -\tfrac{3}{60}\langle-\tfrac{1}{2}\rangle + \tfrac{6}{60}\langle+\tfrac{3}{2}\rangle$$
$$I^1(+\tfrac{3}{2}) = -\tfrac{1}{60}\langle+\tfrac{1}{2}\rangle + \tfrac{10}{60}\langle+\tfrac{5}{2}\rangle \tag{9}$$
$$I^2(-\tfrac{3}{2}) = \tfrac{10}{60}\langle-\tfrac{5}{2}\rangle - \tfrac{8}{60}\langle-\tfrac{3}{2}\rangle + \tfrac{1}{60}\langle-\tfrac{1}{2}\rangle$$
$$I^2(-\tfrac{1}{2}) = \tfrac{6}{60}\langle-\tfrac{3}{2}\rangle - \tfrac{12}{60}\langle-\tfrac{1}{2}\rangle + \tfrac{3}{60}\langle+\tfrac{1}{2}\rangle$$
$$I^2(+\tfrac{1}{2}) = \tfrac{3}{60}\langle-\tfrac{1}{2}\rangle - \tfrac{12}{60}\langle+\tfrac{1}{2}\rangle + \tfrac{6}{60}\langle+\tfrac{3}{2}\rangle$$
$$I^2(+\tfrac{3}{2}) = \tfrac{1}{60}\langle+\tfrac{1}{2}\rangle - \tfrac{8}{60}\langle+\tfrac{3}{2}\rangle + \tfrac{10}{60}\langle+\tfrac{5}{2}\rangle. \tag{10}$$
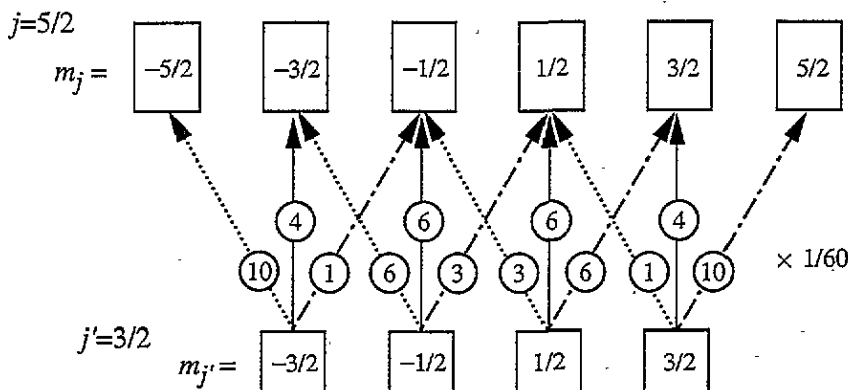
Figure 1. Dipole transitions for x-ray absorption from a $j' = 3/2$ core level to an open shell $j = 5/2$. The components m_j of each level are shown as boxes. The transition probabilities (encircled numbers) for excitation with left circularly ($\Delta m_j = -1$), Z perpendicularly ($\Delta m_j = 0$) and right circularly ($\Delta m_j = +1$) polarized light of an electron from the filled level to the incompletely filled level are indicated by dotted, full and dash–dotted lines, respectively.

In x-ray absorption we cannot resolve the different $m_{j'}$ sublevels and we measure only

the sum of the intensities, designated by the superscript $r = 0$

$$I^{a(r=0)} = I^a(-\tfrac{3}{2}) + I^a(-\tfrac{1}{2}) + I^a(+\tfrac{1}{2}) + I^a(+\tfrac{3}{2}). \qquad (11)$$

Because each absorbed photon creates a hole in the core level we may say that each spectrum I^a creates a distribution of holes in the $m_{j'}$ levels which again can be described in a statistical way in terms of multipole moments r of the core hole. So in x-ray absorption we detect $r = 0$ which is the monopole or the spherical part of the core hole or simply the number of core holes, cf (2). Substitution of (8)–(10) into (11) gives

$$I^{0(r=0)} = \tfrac{10}{60}\langle-\tfrac{5}{2}\rangle + \tfrac{10}{60}\langle-\tfrac{3}{2}\rangle + \tfrac{10}{60}\langle-\tfrac{1}{2}\rangle + \tfrac{10}{60}\langle+\tfrac{1}{2}\rangle + \tfrac{10}{60}\langle+\tfrac{3}{2}\rangle + \tfrac{10}{60}\langle+\tfrac{5}{2}\rangle = \tfrac{1}{6}\langle w^0\rangle \qquad (12)$$

$$I^{1(r=0)} = -\tfrac{10}{60}\langle-\tfrac{5}{2}\rangle - \tfrac{6}{60}\langle-\tfrac{3}{2}\rangle - \tfrac{2}{60}\langle-\tfrac{1}{2}\rangle + \tfrac{2}{60}\langle+\tfrac{1}{2}\rangle + \tfrac{6}{60}\langle+\tfrac{3}{2}\rangle + \tfrac{10}{60}\langle+\tfrac{5}{2}\rangle = \tfrac{1}{6}\langle w^1\rangle \qquad (13)$$

$$I^{2(r=0)} = \tfrac{10}{60}\langle-\tfrac{5}{2}\rangle - \tfrac{2}{60}\langle-\tfrac{3}{2}\rangle - \tfrac{8}{60}\langle-\tfrac{1}{2}\rangle - \tfrac{8}{60}\langle+\tfrac{1}{2}\rangle - \tfrac{2}{60}\langle+\tfrac{3}{2}\rangle + \tfrac{10}{60}\langle+\tfrac{5}{2}\rangle = \tfrac{1}{6}\langle w^2\rangle. \qquad (14)$$

Summarizing, when we measure the monopole of the core hole produced by a polarized light we measure a ground state multipole expectation value

$$I^{a(r=0)} = \tfrac{1}{6}\langle w^a\rangle \qquad (15)$$

which is the equivalent of the XAS sum rules for the $j = \tfrac{3}{2}$ edge [7,8].

This paper deals with the higher multipole moments of the core hole, which can be measured if we consider an autoionization process where the deep core hole decays to a shallower two-hole state under emission of an electron into the continuum state e. The Coulomb matrix element which is responsible for the decay conserves the total magnetic moment so that

$$m_{j'} + m_e = m_p + m_d \qquad (16)$$

where m_p and m_d are the magnetic moments of the two final state holes. Now the value of $m_p + m_d$ is restricted by the final state term of the ionic configuration which, as we assume, can be resolved in energy. E.g. for a $J = 0$ final state $m_p + m_d = 0$. Further the *absolute value* of m_e can be determined from the angular distribution of the photoemission. This means that $m_{j'} = \pm\tfrac{3}{2}$ can be separated from $m_{j'} = \pm\tfrac{1}{2}$ and we see that we can now measure the *quadrupole moment* $r = 2$ of the core hole defined as

$$I^{a(r=2)} = I^a(-\tfrac{3}{2}) - I^a(-\tfrac{1}{2}) - I^a(+\tfrac{1}{2}) + I^a(+\tfrac{3}{2}). \qquad (17)$$

Substitution of (8)–(10) into (17) gives

$$I^{0(r=2)} = \tfrac{10}{60}\langle-\tfrac{5}{2}\rangle - \tfrac{2}{60}\langle-\tfrac{3}{2}\rangle - \tfrac{8}{60}\langle-\tfrac{1}{2}\rangle - \tfrac{8}{60}\langle+\tfrac{1}{2}\rangle - \tfrac{2}{60}\langle+\tfrac{3}{2}\rangle + \tfrac{10}{60}\langle+\tfrac{5}{2}\rangle = \tfrac{1}{6}\langle w^2\rangle \qquad (18)$$

$$I^{1(r=2)} = -\tfrac{10}{60}\langle-\tfrac{5}{2}\rangle + \tfrac{6}{60}\langle-\tfrac{3}{2}\rangle + \tfrac{4}{60}\langle-\tfrac{1}{2}\rangle - \tfrac{4}{60}\langle+\tfrac{1}{2}\rangle - \tfrac{6}{60}\langle+\tfrac{3}{2}\rangle + \tfrac{10}{60}\langle+\tfrac{5}{2}\rangle$$
$$= \tfrac{1}{15}\langle w^1\rangle + \tfrac{1}{60}\langle w^3\rangle \qquad (19)$$

$$I^{2(r=2)} = \tfrac{10}{60}\langle-\tfrac{5}{2}\rangle - \tfrac{14}{60}\langle-\tfrac{3}{2}\rangle + \tfrac{10}{60}\langle-\tfrac{1}{2}\rangle + \tfrac{10}{60}\langle+\tfrac{1}{2}\rangle - \tfrac{14}{60}\langle+\tfrac{3}{2}\rangle + \tfrac{10}{60}\langle+\tfrac{5}{2}\rangle$$
$$= \tfrac{1}{30}\langle w^0\rangle + \tfrac{1}{21}\langle w^2\rangle + \tfrac{3}{35}\langle w^4\rangle. \qquad (20)$$

This shows that we have obtained information on $\langle w^3\rangle$ and $\langle w^4\rangle$.

If we measure the spin of the emitted electron we can also separate $m_{j'}$ and $-m_{j'}$ and so obtain odd core hole multipoles, which give again different combinations of 3d shell multipoles. Thus with core polarization we obtain additional information about the moments of the ground state.

The foregoing explanation was given in a simple jj coupling language. In order to treat core hole polarization in a general way we will in section 3 apply the diagrammatic methods of Yutsis *et al* [67–69], using essentially the same approach, to determine the expectation values of coupled tensor operators $\langle w^{xyz}\rangle$ as defined in appendix A from the

intensity and spin distributions of final state peaks in various regimes of Coulomb and spin–orbit interaction, LS, LSJ and jjJ coupling. We will obtain an expression for the angle and spin dependent intensity as a sum over the tensor operators w^{xyz}, multiplied by C^{xyzar}, which is the probability of creating a core hole with moment r for a given ground state xyz using a polarized light, multiplied by B, which is the probability of decay of a core hole with moment r into the final state, multiplied by the angular distribution U, by which we can recognize the outgoing electron.

3. Theory

3.1. Decomposition in excitation and decay

Our approach in this paper is to decompose the core–core–core resonant photoemission intensity in such a way that it can be interpreted as a process in which first an excitation is made from a core level to the valence shell, leaving behind a non-spherical core hole. After this the core hole decays to two shallower core holes in a specific state, which can be selected by the energy of the emitted photoelectron. The non-spherical nature of the core hole together with the properties of the selected final state then cause a specific spatial and spin distribution of the emitted electron.

We will consider the resonant photoemission process consisting of a Q-pole absorption from a ground state $|g\rangle$ to a set of intermediate states $|i\rangle$ followed by the decay into final states $|f\rangle$ plus a continuum electron. The state $|g\rangle$ has all core levels filled and has a localized shell l only partly filled, such as the 3d level of transition metal compounds or the 4f level of rare earth materials (see figure 2). In the text we will for brevity often refer to 3d transition metal compounds. The states $|i\rangle$ treated here have one electron transferred from a deep core level c, say 2p, to the 3d level. The c level has a large spin–orbit splitting and we will consider transitions from the two levels $j = c \pm \frac{1}{2}$ separately. The final states $|f\rangle$ have the deep core level filled and two holes in other, shallower core levels, such as both in 3p or one in 3p and one in 3s. We can designate these processes as $2p_{3/2}3p3p$ and $2p_{3/2}3p3s$ decay, respectively. In transition metal ions the shallow core levels, designated in the following by p and d, have a large Coulomb interaction and so the final states are split into well separated groups corresponding to different LS terms of the $\underline{pd}$ configuration. These terms are smeared out somewhat by the presence of the l shell but we will assume that this effect is small enough to consider the core hole LS character as approximately pure. In heavier atoms the final state core levels can also have large spin–orbit splitting and may be described more properly by LSJ coupling or even by $j_p j_d J$ coupling such as in the 2p3p3p decay of rare earth ions.

The electric Q-pole transition matrix element from the c_j level to the l level is given by

$$\sum_{12} \langle i|l_1^\dagger j_2|g\rangle \quad \overset{1}{\underset{2}{\diagdown}}{\overset{j}{\underset{c}{\diagup}}}^{2}_{1} \quad [jcl]^{1/2} \tag{21}$$

where we have used $1, 2, \ldots$ to denote the components $m_{1,2,\ldots}$ and $\sigma_{1,2,\ldots}$ of the momenta l, j, etc. Whether m, σ or both is meant is always clear from the context. A line on a graph without a moment specified refers to $s = \frac{1}{2}$. Finally $[a, b, \ldots]$ is shorthand for $(2a + 1)(2b + 1)\ldots$. To obtain elegant tables we have omitted the radial integral and a coefficient n_{cQl} defined in (A5).

The decay matrix element is due to Coulomb interaction with a continuum level. The k-pole Coulomb matrix element for decay to a continuum level with symmetry e, with the
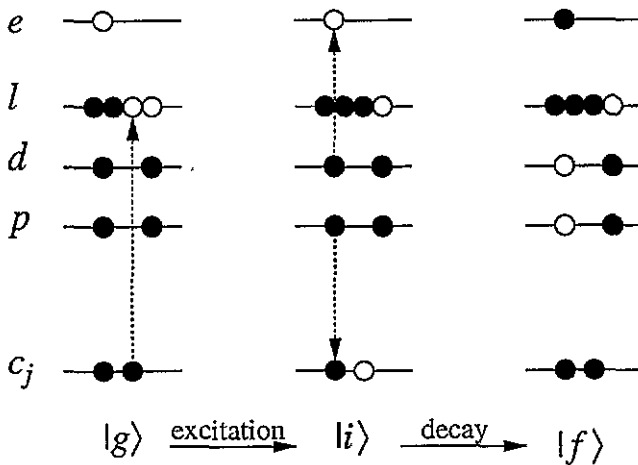
Figure 2. The autoionization or resonant photoemission process. In the x-ray absorption process a core electron in the level c_j is excited into an open shell l. The resulting intermediate state $|i\rangle$ decays by Coulomb interaction to a two-hole final state under emission of a photoelectron into the continuum state e. .

electron measured in direction ε leaving behind the ion in state $|f\rangle$ is

$$\sum_{3456ke} \langle f|j_3^\dagger d_4 p_6|i\rangle Y_{m_s}^e(\varepsilon) \qquad [jcpde]^{1/2}(-)^{p+k+d} n_{ekp} n_{ckd} R_{cpde}^k \, e^{i\delta_e} \qquad (22)$$

where R_{cpde}^k are the radial integrals, δ_e is the phase shift of e, and $Y_{m_s}^e$ is a spherical harmonic. (22) should also contain exchange terms with p and d interchanged. The behaviour of these terms is exactly analogous in the derivation so we will leave them out but include them in the end result.

3.2. The removal of the core operators

Taking the square of the product of (21) and (22) we obtain for the creation/annihilation part of the intensity

$$\sum_{ii'1234\underline{6}1\underline{2}3\underline{4}6} \langle g|j_{\underline{2}}^\dagger l_{\underline{1}}|i'\rangle\langle i'|p_{\underline{6}}^\dagger d_{\underline{4}}^\dagger j_{\underline{3}}|f\rangle\langle f|j_3^\dagger d_4 p_6|i\rangle\langle i|l_1^\dagger j_2|g\rangle \qquad (23)$$

where as a convention the moments $\underline{1}, \underline{2}, \dots$ in the Hermitian conjugate part correspond to $1, 2, \dots$. Here $|i\rangle$ denotes only states with a c_j hole but we can extend the summation over i to all states in the Hilbert space and use the closure relation because states without a c_j hole give only terms that are zero. In the total expression for the intensity there is an energy denominator involving i and i'. The consequences of neglecting this will be discussed in section 4. We can now use

$$\langle f|j_3^\dagger \dots j_2|g\rangle = \langle f| \dots |g\rangle \delta_{23} \qquad (24)$$

and obtain

$$\langle g|l_{\underline{1}} p_{\underline{6}}^\dagger d_{\underline{4}}^\dagger|f\rangle\langle f|d_4 p_6 l_1^\dagger|g\rangle \delta_{23}\delta_{\underline{2}\underline{3}}. \qquad (25)$$

In this way we have restricted our intensity to excitation and decay via the selected c_j states. We may say that we have disposed of the presence of the open l shell in the intermediate states by summing over all structure in the c_j edge caused by cl Coulomb interactions. So after being inspected by the Pauli principle the l shell is treated as a spectator in the rest of the process. In a similar manner we can restrict the intensity to that of all final state levels belonging to e.g. a selected LS term of the pd configuration, irrespective of the state of the spectator l shell. For this we sum over all $\overline{|f\rangle}$ which have pd holes in states belonging to this term. These $|f\rangle$ can be written as

$$|f L M_L S M_S\rangle \equiv \sum_{\underline{78}} \ \ [LS]^{1/2} d_{\underline{7}} p_{\underline{8}} |f_0\rangle \tag{26}$$

where we let $|f_0\rangle$ run over all states without any holes in p or d. But, again we can include the p and d hole states in the summation after substitution into (25) because the hole state terms give zero. Furthermore, because $|g\rangle$ also contains no core holes we have

$$\langle f_0| p_{\underline{8}}^\dagger d_{\underline{7}}^\dagger d_4 p_6 l_1|g\rangle = \delta_{68}\delta_{47}\langle f_0|l_1|g\rangle \tag{27}$$

and we obtain

$$\sum_{M_L M_S} \langle g|l_{\underline{1}} l_{\underline{1}}^\dagger|g\rangle \ \ [LS]$$

$$= \langle g|l_{\underline{1}} l_{\underline{1}}^\dagger|g\rangle \ \ [LS]. \tag{28}$$

The result is a one-electron expectation value for $|g\rangle$, taking the place of the density matrix or statistical tensor in atomic theory. Completing the expression and connecting the graphs by the summation over $\underline{246246}$ using the δ factors gives

$$\sum_{\underline{11}} \langle g|l_{\underline{1}} l_{\underline{1}}^\dagger|g\rangle \ \ R^k_{cpde} R^k_{cp d\underline{e}} \, e^{i(\delta_\varepsilon - \delta_\varepsilon)} \frac{1}{4\pi} [jclLSjcpde\underline{e}] n_{ekp} n_{dkc} n_{ck\underline{d}} n_{pk\underline{e}}. \tag{29}$$

The double bars denote normalized spherical harmonics. In order to obtain the expression for the intensity of the fundamental spectra for light polarized along P and spin polarization measured along P_S, we multiply by $r^{sh}_{\sigma s \sigma_{\underline{s}}}(P_S)$ and $r^{Qa}_{q\underline{q}}(P)$ defined in paper III, equation (5) as

$$r^{Qa}_{qq'}(P) \equiv n_{Qa}^{-1} \qquad = \sum_\alpha n_{Qa}^{-1} C_\alpha^a(P)(-)^{Q-q} \begin{pmatrix} Q & a & Q \\ -q & a & q' \end{pmatrix} \tag{30}$$

and use

$$\sum_b [b] \qquad = \qquad [b] n_{eb\underline{e}}. \tag{31}$$

The result is

$$J_j^{ah}(LS; PP_S\varepsilon) = \frac{1}{4\pi} \sum_{1\underline{1}b} \sum_{kk\underline{e}\underline{e}} \langle g|l_1 l_1^\dagger|g\rangle \qquad R_{cpde}^k R_{cpd\underline{e}}^k e^{i(\delta_\varepsilon - \delta_{\underline{\varepsilon}})}$$
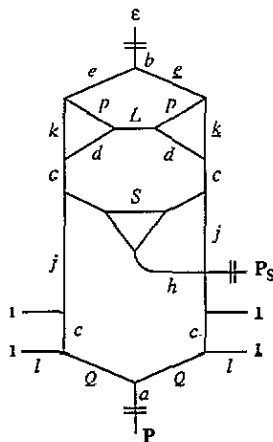
$$\times [jcl\,LSj\,cpd\,e\underline{e}b]n_{Qa}^{-1}n_{ekp}n_{dkc}n_{ckd}n_{pk\underline{e}}n_{eb\underline{e}}n_{sh}^{-1}. \tag{32}$$

3.3. The excitation step

At this point we see that the problem can be divided naturally into two separate pieces. The first part, going from Q to j in the graph, expresses the dipole excitation from the ground state to the states with c_j holes; the other part gives the decay into the final states by Coulomb interaction. This separation can be made by summing over an extra quantum number r, the multipole of the core hole.

$$\tag{33}$$

The excitation part gives

$$\equiv \sum_{xyz\zeta} \langle w_\zeta^{xyz}\rangle n_{zar}^{-1} \qquad C_j^{xyzar}. \tag{34}$$

This tells us that given a ground state with moment xyz the dipole transition creates a core hole with moments r with probabilities C. The origin of this effect is the Pauli principle which allows the core electron to go into a valence level only if it is empty. Thus the absorption step probes the occupation of the valence levels and, depending also on the polarization of the light a, it can create only specific core holes, leaving a non-spherical core shell. The spin of the ground state ($y = 1$) comes in through the spin–orbit coupling of the core level. This has the effect that in order to excite an electron with a certain spin into l, it must have an appropriate orbital part, i.e. parallel or antiparallel to the spin for

$j = c \pm 1/2$ respectively. This produces the anisotropy of the hole orbital. The coefficient C can be decomposed by introduction of an extra summation variable α, the *orbital* multipole of the core level.

$$
C_j^{xyzar}(lcQ) = \sum_\alpha \begin{Bmatrix} j & r & j \\ s & y & s \\ c & \alpha & c \end{Bmatrix} \begin{Bmatrix} x & y & z \\ r & a & \alpha \end{Bmatrix} \begin{Bmatrix} c & \alpha & c \\ l & x & l \\ Q & a & Q \end{Bmatrix}
$$
$$
\times [\alpha j c l x y z] n_{lx} n_{sy} n_{xyz} n_{zar} n_{Qa}^{-1} n_{jr}^{-1}. \tag{35}
$$

3.4. The decay step

3.4.1. LS coupling. The upper part of the diagram in (32) gives the probability distribution for emission of an electron by the decay of the core hole with moment r to a state with two other core holes forming a state LS. The distribution is caused by the fact that one electron has to fall into the polarized core hole while the emitted electron has to leave behind a core hole of the right type of orbital and spin so that together the remaining holes form the required LS level.

$$ \tag{36} $$
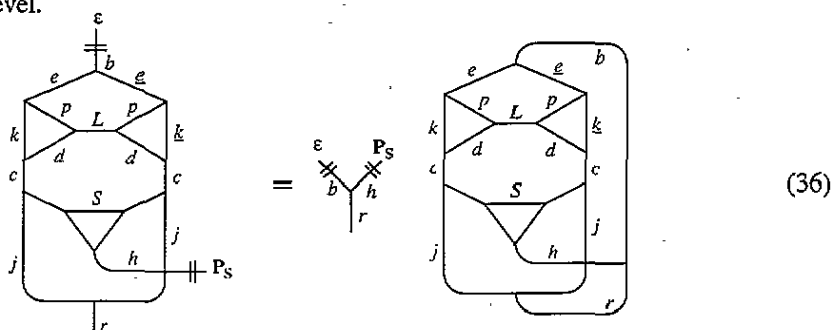
The total expression for the angle and spin dependent emission intensity J_j^{ah} from the edge with total angular momentum j using polarized light of moment a and detecting the photoelectron spin of moment h for transition from a core state to the LS term of the two-core-hole state can be written as

$$
J_j^{ah}(LS; PP_S\varepsilon) = \frac{1}{4\pi} \sum_{zrb\zeta} \left\{ \sum_{xy} \langle \underline{w}_\zeta^{xyz} \rangle C_j^{xyzar} \right\} U_\zeta^{zarhb}(PP_S\varepsilon) B_j^{rhb}(LS) \tag{37}
$$

where the angle dependence is
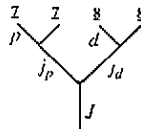
$$
U_\zeta^{zarhb}(PP_S\varepsilon) = \begin{array}{c} \text{(diagram)} \end{array} \quad n_{zar}^{-1} n_{rhb}^{-1} \tag{38}
$$

and from (36) the coefficient B for the probability that a core hole with moment r decays into the state LS and a photoelectron with orbital moment b and spin moment h is

$$
B_j^{rhb}(LS) = \begin{Bmatrix} c & b & c \\ s & h & s \\ j & r & j \end{Bmatrix} \begin{Bmatrix} s & h & s \\ s & S & s \end{Bmatrix}
$$
$$
\times \sum_{e\underline{e}} \begin{Bmatrix} e & b & \underline{e} \\ c & L & c \end{Bmatrix} e^{j(\delta_e - \delta_{\underline{e}})} \sum_k \begin{Bmatrix} e & k & p \\ d & L & c \end{Bmatrix} R_{cpde}^k \sum_{\underline{k}} \begin{Bmatrix} p & \underline{k} & \underline{e} \\ c & L & d \end{Bmatrix} R_{cpd\underline{e}}^{\underline{k}}
$$
$$
\times (-)^{L+S} [LSjrcpde\underline{eb}] n_{jr} n_{ekp} n_{dkc} n_{ck\underline{d}} n_{pk\underline{e}} n_{eb\underline{e}} n_{sh}^{-1} \underline{n}_{bhr}. \tag{39}
$$

Each summation of k in this expression is understood to contain also the term where p and d are interchanged together with a sign $(-)^{L+S}$. One minus sign is needed because

the annihilation operators in (22) also have to be interchanged, $(-)^{L+S+2s}$ because the final state definition in (26) differs by this sign if we interchange p and d.

Because the $9j$-symbol has two equal columns $b+h+r$ must be even. The expression is symmetric under interchange of e and $\underline{e}$ except for the phase shift factor which is complex conjugated. So the total is real and $e^{i(\delta_e - \delta_{\underline{e}})}$ may be replaced by $\cos(\delta_e - \delta_{\underline{e}})$.

(37) together with (35), (38) and (39) is our main result for LS coupling and can also be expressed in other couplings as shown in the remainder of this section.

3.4.2. LSJ coupling.
When one or both of the two final state holes have appreciable spin–orbit coupling it may be possible to separate the different J levels of the LS term. The result is derived in the same way but in (36) we replace

$$\frac{L}{S} \rightarrow \sum_J [J] \quad \begin{array}{c} L \quad J \quad L \\ \diagdown \\ S \quad \quad S \end{array} \tag{40}$$

and so we obtain

$$(41)$$

This graph is decomposed naturally by introducing the extra moments j_e and $j_{\underline{e}}$, effectively coupling the orbital and spin of the outgoing electron to a total moment

$$B_j^{rhb}(LSJ) = \sum_{e\underline{e}} \sum_{j_e j_{\underline{e}}} \begin{Bmatrix} L & c & e \\ S & s & s \\ J & j & j_e \end{Bmatrix} \begin{Bmatrix} e & b & \underline{e} \\ s & h & s \\ j_e & r & j_{\underline{e}} \end{Bmatrix} \begin{Bmatrix} \underline{e} & c & L \\ s & s & S \\ j_{\underline{e}} & j & J \end{Bmatrix} \begin{Bmatrix} j & r & j \\ j_e & J & j_{\underline{e}} \end{Bmatrix} e^{i(\delta_e - \delta_{\underline{e}})}$$

$$\times \sum_k \begin{Bmatrix} e & k & p \\ d & L & c \end{Bmatrix} R_{cpde}^k$$

$$\times \sum_{\underline{k}} \begin{Bmatrix} p & k & \underline{e} \\ c & L & d \end{Bmatrix} R_{cpd\underline{e}}^{\underline{k}} (-)^{L+S} [LSJjrj_e j_{\underline{e}} cpde\underline{e}b]$$

$$\times n_{jr} n_{ekp} n_{dkc} n_{ckd} n_{pk\underline{e}} n_{eb\underline{e}} n_{sh}^{-1} \underline{n}_{bhr}. \tag{42}$$

Interchange of e, j_e with $\underline{e}$, $j_{\underline{e}}$ changes the product of the three $9j$-symbols by $(-)^{b+h+r}$. So for $b+h+r$ even we may replace the exponential by $\cos(\delta_e - \delta_{\underline{e}})$. For $b+h+r$ odd this is $-i\sin(\delta_e - \delta_{\underline{e}})$. The $-i$ is cancelled by the i in $\underline{n}_{bhr}$. This means that $b+h+r$ odd is allowed in LSJ coupling provided there are terms with $e \neq \underline{e}$ in the summation, in other words there is interference between the continuum channels e and $\underline{e}$.

3.4.3. jjJ coupling.
When both final state core holes have a spin–orbit coupling larger than their Coulomb interaction the observed final states may be described more appropriately

as jjJ states

$$|fj_p j_d J\rangle = \sum_{\underline{78}} p_{\underline{7}} d_{\underline{8}} |f_0\rangle \qquad (43)$$

We now obtain for the decay graph

$$(44)$$

which again can be decomposed by coupling to j_e and $j_{\underline{e}}$, yielding

$$
\begin{aligned}
B_j^{rhb}(j_p j_d J) = \sum_{e\underline{e}} \sum_{j_e j_{\underline{e}}} &\begin{Bmatrix} e & b & \underline{e} \\ s & h & s \\ j_e & r & j_{\underline{e}} \end{Bmatrix} \begin{Bmatrix} j & r & j \\ j_e & J & j_{\underline{e}} \end{Bmatrix} \\
&\times e^{i(\delta_e - \delta_{\underline{e}})} \sum_k R^k \begin{Bmatrix} e & k & p \\ j_p & s & j_e \end{Bmatrix} \begin{Bmatrix} d & k & c \\ j & s & j_d \end{Bmatrix} \begin{Bmatrix} j_p & k & j_e \\ j & J & j_d \end{Bmatrix} \\
&\times \sum_{\underline{k}} R^{\underline{k}} \begin{Bmatrix} \underline{e} & \underline{k} & p \\ j_p & s & j_{\underline{e}} \end{Bmatrix} \begin{Bmatrix} d & \underline{k} & c \\ j & s & j_d \end{Bmatrix} \begin{Bmatrix} j_p & \underline{k} & j_{\underline{e}} \\ j & J & j_d \end{Bmatrix} \\
&\times (-)^{c+J+e+s+j_e} [j_p j_d J j r j_e j_{\underline{e}} c p d e e b] n_{jr} n_{ekp} n_{dkc} n_{\underline{ckd}} n_{\underline{pke}} n_{eb\underline{e}} n_{sh}^{-1} \underline{n}_{bhr}. \qquad (45)
\end{aligned}
$$

Interchange of e, j_e with $\underline{e}$, $j_{\underline{e}}$ changes the $9j$-symbol together with the factor $(-)^{e+s+j_e}$ again by $(-)^{b+h+r}$ and so the same situation occurs as in LSJ coupling with respect to interference. In the summation over k there are again exchange terms where p and d are interchanged and the term is multiplied by $(-)^J$.

4. Interference

In order to discuss the validity of our approach in section 3 we will study the general formula for second-order processes. We are especially interested in the interference effects that influence our results. We will not have to treat interference with direct photoemission which is not possible for a two-core hole final state.

The general formula is

$$I(\omega, E_b) = \sum_{fii'} \frac{\langle g|T|i'\rangle \langle i'|V|f\rangle \langle f|V|i\rangle \langle i|T|g\rangle}{(E_{i'} - E_g - \omega + i\Gamma_{i'}/2)(E_i - E_g - \omega - i\Gamma_i/2)} \delta(E_f - E_g - E_b) \qquad (46)$$

where $E_b = \omega - E_e$ is the binding energy, E_e is the energy of the emitted electron, i and f denote the intermediate and final states with energies E_i and E_f respectively, T is the dipole operator and V is the Coulomb operator responsible for the decay (see figure 3). The denominator prevents independent summation over i and i' because it allows only terms ii' where $E_i - E_{i'} \lesssim \Gamma_i$. The δ-factor does not enter our discussion and we remove it by

considering the intensity integrated at constant ω over an E_b range containing a set of states $\{f\}$ of interest to us, preferably well separated from the rest of the spectrum, because the intermediate states are the *degenerate* M_L, M_S or M_J levels.

$$I_{\{f\}}(\omega) = \int_{\{f\}} dE_b \, I(\omega, E_b) = \sum_{\{f\}ii'} \frac{T_{gi'}V_{i'f}V_{fi}T_{ig}}{(E_{i'} - E_g - \omega + i\Gamma_{i'}/2)(E_i - E_g - \omega - i\Gamma_i/2)} \tag{47}$$

where we have used shorthand for the matrix elements in the numerator. In core level spectroscopy the variation in E_i can be neglected with respect to $E_i - E_g$ and therefore to remove the denominator we would like to replace $E_{i'}$ by E_i and obtain

$$I_{\{f\}}(\omega) = \sum_{\{f\}ii'} \frac{T_{gi'}V_{i'f}V_{fi}T_{ig}}{(E_i - E_g - \omega)^2 + \Gamma_i^2/4}. \tag{48}$$

This is a good approximation if in the summation over ii' the only large numerators occur for terms with $E_i - E_{i'}$ much smaller than Γ_i and $\Gamma_{i'}$. We may say that there is path from g to f via i when T_{gi} and V_{if} are both large. Then (48) is a good approximation when there are no two paths from g to f with energy difference larger than Γ. If there are such paths (48) will contain cross-terms that are absent in reality. If (48) holds we can integrate ω over a range containing a set of states $\{i\}$ well separated from other peaks and obtain

$$I_{\{f,i\}} = \sum_{\{f\}} I_{\{f\}}(\omega) \, d\omega = \sum_{\{ii'f\}} \frac{2\pi}{\Gamma} T_{gi'}V_{i'f}V_{fi}T_{ig}. \tag{49}$$
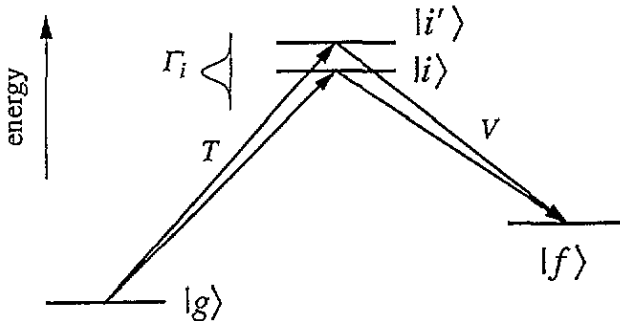
Figure 3. The two-step model breaks down when the intermediate states $|i\rangle$ and $|i'\rangle$ can both be reached in the absorption step from the same ground level and decay to the same final state $|f\rangle$, having an energy separation larger than their natural width Γ_i.

We can now state our basic assumption more precisely: (48) is a good approximation if in the range $\{i\}$ there are no states i and i' forming a path from g to the same f and having energies differing by more than Γ.

The interference problem is absent from gas phase experiments where atomic theory can be used, if we can find an intermediate LS or LSJ term which is well separated from rest of the spectrum, because the intermediate states are the degenerate $M_L M_S$ or M_J levels.

(48) is also exact in one-particle theory, where i denotes states with a core hole and with an extra valence electron in level v_i. Then the levels i are not degenerate but $V_{if}V_{fi'}$ connects only states with the same energy because the v level has no interaction with the core holes in i or f and so is a pure spectator in the decay: $v_i = v_{i'}$. Therefore, deviations from (48) may be useful in the study of the validity of the one-particle theory in the presence of core–valence interactions. The presence of valence–valence interactions has no consequence because without core–valence interactions the whole many-electron valence shell is still only a spectator to the purely core decay.

5. Final state characteristics

We consider here characteristics of final states that simplify the interpretation of spectra. We designate a general decay channel by $l_1 l_2 l_3 e$. The intermediate state only has a hole in l_1 and so its total orbital moment is l_1. The final state consists of two holes in l_2 and l_3 coupled to L and together with the continuum electron the total orbital moment has the possible values $L_{tot} = L \otimes e = |L - e| \cdots L + e$. The decay is only possible when $L_{tot} = l_1$, or equivalently

$$e = L \otimes l_1 = |L - l_1| \cdots L + l_1. \tag{50}$$

The final state L values are $l_2 \otimes l_3 = |l_2 - l_3| \cdots l_2 + l_3$ but there is an extra restriction on e: due to the parity of the Coulomb interaction $l_1 + l_2 + l_3 + e$ must be even. The possible values of e are therefore

$$e = l_1 + l_2 + l_3, l_1 + l_2 + l_3 - 2, \ldots, \max(l_1 - l_2 - l_3, l_2 - l_3 - l_1, l_3 - l_2 - l_1, 0). \tag{51}$$

Let us now consider whether there are decays involving L values that can only be reached for one e. In those decays there are no interference terms arising as cross-terms between different e channels. If we consider first those L values that are equal to a possible value of e from (51), then with $l_1 = 0$ obviously by (50) those L can only be reached in one decay channel: $e = L$. But also with $l_1 = 1$ only $e = L$ will contribute, because $e = L - 1$ and $e = L + 1$ have the wrong parity. Another case occurs when $l_2 = l_3$ where we have a term with $L = 0$, which means $e = l_1$ only.

For jjJ coupling the only case with one continuum channel seems to be $J = 0$. Because of the triad $(jj_e J)$ we must have $j_e = j$ and $e = j_e \pm \frac{1}{2}$ but only the value with the right parity is allowed.

These simple cases will only be of any value if the peak with the desired L or J value is sufficiently separated from the rest of the final states. When the Coulomb interactions are not very large this will only be so for a high-spin state with a high L value, because such a state is often split off at the low-energy side of the configuration. Likewise, in jjJ coupling the Coulomb interactions have to be large enough to split the J levels but this will probably be true due to the large Coulomb interactions between deep core levels. Of course in order to measure with odd $h + r$ (cf section 6) we have to avoid these non-interfering states.

Another point is configuration interaction of the two-core-hole final state with nearby configurations [24, 25]. This is important in transition metal ions where the configuration $3p^4 d^n e$ is close enough to $3s^1 d^{n-1} e$ to complicate the analysis. In such cases there may however be LS terms that are not present in the undesired configuration. In the example only ^1D is present in both configurations, leaving ^3P and ^1S free from both interference and configuration interaction. In those cases the polarization and angle dependence does not depend on any parameters such as Coulomb matrix elements and phase factors. This situation is desirable if we are not interested in the final states themselves but only in their use as a probe of the intermediate state core hole polarization which in turn probes the valence shell.

6. Analysis

6.1. The excitation process

The important characteristics of the experiment are which type of moment, magnetic or non-magnetic, is being measured, whether linearly or circularly polarized light and/or spin

Table 1. The linear combinations of moments $\langle \underline{w}^{xyz}\rangle$ for p to d excitations with a polarized light and core hole moment r. For even r the corresponding angle dependent function is U^{zar} which implies spin unpolarized measurement. For odd r spin polarized measurement is necessary, with angle dependent functions U^{zar1b} with $b = r - 1$ and $b = r + 1$. In the presence of spin–orbit coupling in the final state and interference between continuum channels, even r can also be studied by measurement of U^{zar1r}.

zar	$\sum_{xy} C_{3/2}^{xyzar} \underline{w}^{xyz}$	$\sum_{xy} C_{1/2}^{xyzar} \underline{w}^{xyz}$
000	$2\underline{w}^{000} + \underline{w}^{110}$	$\underline{w}^{000} - \underline{w}^{110}$
011	$\frac{1}{9}(5\underline{w}^{000} + 4\underline{w}^{110})$	$\frac{1}{3}(\underline{w}^{000} - \underline{w}^{110})$
022	$\frac{1}{5}(\underline{w}^{000} + 2\underline{w}^{110})$	
101	$\frac{1}{9}(10\underline{w}^{011} + 15\underline{w}^{101} + 2\underline{w}^{211})$	$\frac{1}{3}(-\underline{w}^{011} + 3\underline{w}^{101} - 2\underline{w}^{211})$
110	$\frac{1}{3}(\underline{w}^{011} + 6\underline{w}^{101} + 2\underline{w}^{211})$	$\frac{1}{3}(-\underline{w}^{011} + 3\underline{w}^{101} - 2\underline{w}^{211})$
112	$\frac{2}{15}(5\underline{w}^{011} + 3\underline{w}^{101} + \underline{w}^{211})$	
121	$\frac{2}{45}(\underline{w}^{011} + 15\underline{w}^{101} + 11\underline{w}^{211})$	$\frac{2}{15}(-\underline{w}^{011} + 3\underline{w}^{101} - 2\underline{w}^{211})$
123	$\frac{3}{35}(7\underline{w}^{011} + 2\underline{w}^{211})$	
202	$2\underline{w}^{112} + \underline{w}^{202}$	
211	$\frac{2}{45}(17\underline{w}^{112} + 25\underline{w}^{202} + 3\underline{w}^{312})$	$\frac{2}{15}(-2\underline{w}^{112} + 5\underline{w}^{202} - 3\underline{w}^{312})$
213	$\frac{3}{35}(14\underline{w}^{112} + \underline{w}^{312})$	
220	$\frac{1}{5}(2\underline{w}^{112} + 10\underline{w}^{202} + 3\underline{w}^{312})$	$\frac{1}{5}(-2\underline{w}^{112} + 5\underline{w}^{202} - 3\underline{w}^{312})$
222	$\frac{2}{35}(7\underline{w}^{112} + 5\underline{w}^{202} + 3\underline{w}^{312})$	
303	$3\underline{w}^{213}$	
312	$\frac{3}{5}(2\underline{w}^{213} + \underline{w}^{303})$	
321	$\frac{1}{5}(24\underline{w}^{213} + 35\underline{w}^{303} + 4\underline{w}^{413})$	$\frac{3}{35}(-3\underline{w}^{213} + 7\underline{w}^{303} - 4\underline{w}^{413})$
323	$\frac{4}{35}(6\underline{w}^{213} + \underline{w}^{413})$	
413	$\frac{12}{7}\underline{w}^{314}$	
422	$\frac{18}{35}(2\underline{w}^{314} + \underline{w}^{404})$	
523	$\frac{10}{7}\underline{w}^{415}$	

detection are needed and which type of geometry is required. The analysis contains two steps. In the first step an electron is excited to the valence shell by absorption of a photon. The coefficients C give the probability that a moment r is created in the core hole given the moments xyz in the ground state and using a polarized light. We may here consider the light to be polarized along the Z-axis. When it is polarized along another direction the effects are incorporated into the angle dependent function U of (38). The value of a can be 0, 1, 2, and r is in the range $0\ldots 2j$. We have two $9j$-symbols in (35) which require $x + a + \alpha$ and $r + y + \alpha$ both to be even which means $x + y + a + r$ is even. We assume that only moments with even $x + y + z$ are present in the ground state, and so for brevity we will often say that $z + a + r$ must be even. Odd z means a magnetic moment, e.g. L, S or T and even z denotes non-magnetic moments, such as charge multipoles (e.g. monopole and quadrupole) and couplings of odd x and y to an even z, such as spin–orbit coupling (cf appendix A). Even a means isotropic ($a = 0$) or linearly polarized light ($a = 2$) and odd a means circular polarization ($a = 1$). This tells us what values of r are induced in the core hole, especially whether they are even or odd. Even r again means a non-magnetic moment and odd r denotes a magnetic moment. Table 1 gives the values of C for a p to d excitation in the form of the coefficients of $\langle w^{xyz}\rangle$ in the sum over x and y in (37). Table 2 gives the values of C for d to f excitations. We see that naturally we measure linear combinations of the $\langle w^{xyz}\rangle$ but these combinations depend on the values of z, a and r. Formally we may

say that the values of z, a, r, h and b can be chosen by the experimentalist by performing measurements in a number of geometries sufficient to determine all the coefficients of the angle dependence functions U^{zarhb} in (37) and then selecting the combination desired. Assuming the coefficients B to be known, we can determine the linear combinations of $\langle w^{xyz} \rangle$ for a given z in table 1. When we know a sufficient number of these combinations we can solve for the $\langle w^{xyz} \rangle$ separately.

Table 2. The linear combinations of moments $\langle \underline{w}^{xyz} \rangle$ for d to f excitations with a polarized light and core hole moment r. Cf. table 1.

zar	$\sum_{xy} C^{xyzar}_{5/2} \underline{w}^{xyz}$	$\sum_{xy} C^{xyzar}_{3/2} \underline{w}^{xyz}$
000	$3\underline{w}^{000} + 2\underline{w}^{110}$	$2(\underline{w}^{000} - \underline{w}^{110})$
011	$1/15(14\underline{w}^{000} + 11\underline{w}^{110})$	$2/3(\underline{w}^{000} - \underline{w}^{110})$
022	$1/25(12\underline{w}^{000} + 13\underline{w}^{110})$	$2/5(\underline{w}^{000} - \underline{w}^{110})$
101	$1/5(7\underline{w}^{011} + 14\underline{w}^{101} + 4\underline{w}^{211})$	$2/3(-\underline{w}^{011} + 3\underline{w}^{101} - 2\underline{w}^{211})$
110	$1/3(2\underline{w}^{011} + 9\underline{w}^{101} + 4\underline{w}^{211})$	$2/3(-\underline{w}^{011} + 3\underline{w}^{101} - 2\underline{w}^{211})$
112	$2/75(28\underline{w}^{011} + 36\underline{w}^{101} + 11\underline{w}^{211})$	$4/15(-\underline{w}^{011} + 3\underline{w}^{101} - 2\underline{w}^{211})$
121	$2/25(2\underline{w}^{011} + 14\underline{w}^{101} + 9\underline{w}^{211})$	$4/15(-\underline{w}^{011} + 3\underline{w}^{101} - 2\underline{w}^{211})$
123	$9/175(12\underline{w}^{011} + 9\underline{w}^{101} + 4\underline{w}^{211})$	$6/35(-\underline{w}^{011} + 3\underline{w}^{101} - 2\underline{w}^{211})$
202	$1/25(56\underline{w}^{112} + 60\underline{w}^{202} + 9\underline{w}^{312})$	$2/5(-2\underline{w}^{112} + 5\underline{w}^{202} - 3\underline{w}^{312})$
211	$2/75(37\underline{w}^{112} + 70\underline{w}^{202} + 18\underline{w}^{312})$	$4/15(-2\underline{w}^{112} + 5\underline{w}^{202} - 3\underline{w}^{312})$
213	$3/175(72\underline{w}^{112} + 45\underline{w}^{202} + 8\underline{w}^{312})$	$6/35(-2\underline{w}^{112} + 5\underline{w}^{202} - 3\underline{w}^{312})$
220	$1/5(4\underline{w}^{112} + 15\underline{w}^{202} + 6\underline{w}^{312})$	$2/5(-2\underline{w}^{112} + 5\underline{w}^{202} - 3\underline{w}^{312})$
222	$2/175(41\underline{w}^{112} + 60\underline{w}^{202} + 24\underline{w}^{312})$	$4/35(-2\underline{w}^{112} + 5\underline{w}^{202} - 3\underline{w}^{312})$
224	$2/35(18\underline{w}^{112} + 5\underline{w}^{202} + 2\underline{w}^{312})$	
303	$1/35(108\underline{w}^{213} + 63\underline{w}^{303} + 4\underline{w}^{413})$	$2/7(-3\underline{w}^{213} + 7\underline{w}^{303} - 4\underline{w}^{413})$
312	$3/175(79\underline{w}^{213} + 84\underline{w}^{303} + 12\underline{w}^{413})$	$6/35(-3\underline{w}^{213} + 7\underline{w}^{303} - 4\underline{w}^{413})$
314	$4/63(27\underline{w}^{213} + 7\underline{w}^{303} + \underline{w}^{413})$	
321	$3/175(53\underline{w}^{213} + 98\underline{w}^{303} + 24\underline{w}^{413})$	$6/35(-3\underline{w}^{213} + 7\underline{w}^{303} - 4\underline{w}^{413})$
323	$4/525(93\underline{w}^{213} + 63\underline{w}^{303} + 19\underline{w}^{413})$	$8/105(-3\underline{w}^{213} + 7\underline{w}^{303} - 4\underline{w}^{413})$
325	$10/231(33\underline{w}^{213} + 2\underline{w}^{413})$	
404	$4\underline{w}^{314} + \underline{w}^{404}$	
413	$4/315(139\underline{w}^{314} + 81\underline{w}^{404} + 5\underline{w}^{514})$	$8/63(-4\underline{w}^{314} + 9\underline{w}^{404} - 5\underline{w}^{514})$
415	$5/99(44\underline{w}^{314} + \underline{w}^{514})$	
422	$6/175(34\underline{w}^{314} + 36\underline{w}^{404} + 5\underline{w}^{514})$	$4/35(-4\underline{w}^{314} + 9\underline{w}^{404} - 5\underline{w}^{514})$
424	$20/231(11\underline{w}^{314} + 3\underline{w}^{404} + \underline{w}^{514})$	
505	$5\underline{w}^{415}$	
514	$5/9(4\underline{w}^{415} + \underline{w}^{505})$	
523	$2/231(170\underline{w}^{415} + 99\underline{w}^{505} + 6\underline{w}^{615})$	$20/231(-5\underline{w}^{415} + 11\underline{w}^{505} - 6\underline{w}^{615})$
525	$10/429(52\underline{w}^{415} + 3\underline{w}^{615})$	
615	$30/11\underline{w}^{516}$	
624	$5/11(4\underline{w}^{516} + \underline{w}^{606})$	
725	$315/143\underline{w}^{617}$	

The sum rules for x-ray absorption spectroscopy appear in these tables in the guise of sum rules for $r = 0$. XAS measures the total number of core holes created, irrespective of their polarization, and this is exactly what $r = 0$ (monopole) means. For $a = 0$ we see from table 1 that the sum of the C for $j = \frac{3}{2}$ and $j = \frac{1}{2}$ gives $3\langle \underline{w}^{000} \rangle = 3n_h$ and $C_{3/2} - 2C_{1/2} = 3\langle \underline{w}^{110} \rangle = -3\langle l \cdot s \rangle$. For $a = 1$ we get $3\langle \underline{w}^{101} \rangle = \frac{3}{2}\langle L_z \rangle$ and $\langle \underline{w}^{011} \rangle + 2\langle \underline{w}^{211} \rangle = 2\langle S_z \rangle + 7\langle T_z \rangle$ and for $a = 2$ we have $3\langle \underline{w}^{202} \rangle$ and $\frac{6}{5}\langle \underline{w}^{112} \rangle + \frac{9}{5}\langle \underline{w}^{312} \rangle$.

For $j = \frac{1}{2}$ we see first of all that r can only be zero or one and secondly that for each z the linear combination of w operators measured for fixed z but different a and r is the same, except for a constant factor. Further we note that only values of z up to 3 are present.

The operators with $x + y + z$ odd can only be observed for $j = \frac{3}{2}$ but normally in more than one way. The fact that they are not present for $j = c - \frac{1}{2}$ when $c = |l - Q|$ and for $j = c + \frac{1}{2}$ when $c = l + Q$ is not due to triangle relations but to special values for $6j$- and $9j$-symbols for stretched angular momenta [70].

6.2. The decay process

The second step in the process converts the core multipole into final states together with angular distributions and spin polarization of the emitted electron. From (39) we see that if the final states are LS coupled states, i.e. their spin–orbit splitting is not resolved, we have $b + h + r$ even. Because b is always even $h + r$ has to be even. If the spin–orbit splitting in the final state is resolved and at the same time there is interference between different continuum channels the parity of $h + r$ is no longer restricted.

6.3. Geometry and spin dependence

The angle dependent function describes the behaviour of the intensity when the directions of P, P_S and ε are varied. The total set of functions U can describe any angle dependence, but each function has very particular properties. The most important properties are the parities of the moments z, a, r, h and b. The symmetry properties of the total experiment are of course not due to these mathematical entities but due to the physical properties of the system, which are expressed by the values of the coefficients C and B, especially by parity rules for their allowed values. For C these are $z + a + r$ is even and for B we have b is even and in the case of LS coupling of the final states $r + h + b$ is even.

The properties of the functions U in (38) are too complicated to treat in a general way because we have to take into account the symmetry properties of the sample. These are expressed as symmetry restrictions for non-zero $\langle w_\zeta^{xyz} \rangle$. As usual we will restrict ourselves to a sample of cylindrical symmetry where the fact that $\langle w_\zeta^{xyz} \rangle$ must be totally symmetric simply means $\zeta = 0$. In that case we may multiply U by $C_\zeta^z(M)$, which is $\delta_{\zeta 0}$ when M is along the Z-axis, and when we formally sum over ζ we obtain a new function $U^{zarhb}(MPP_S\varepsilon)$ which is now totally symmetric. This means that it does not change if we rotate M, P, P_S and ε together, or equivalently, if we rotate the coordinate axes. This totally symmetric U has simpler properties than the original one. They are described in appendix B.

6.3.1. Spin unresolved measurements.
Figure 4 shows the essential features of the angular distributions $U^{zab}(MP\varepsilon) = U^{zab0b}(MPP_S\varepsilon)$ involved when spin polarization is not detected. The U^{zab} are the same functions as already defined [3] for off-resonance photoemission. However, for resonant photoemission $z + a + b$ can only be even. The plots only show coplanar geometries with M, P and ε in one plane. We see that the value of b determines the number of nodes going around the circle while a determines the difference between the circles. For $a = 0$ the circles are identical because isotropic light has no direction and so the emission intensity cannot depend on P. For linearly polarized light, $a = 2$, the intensity does depend on P, and so the circles become different. The same holds for circularly polarized light, $a = 1$.

6.3.2. Spin polarization: even functions.
First we will consider the case where $r + h + b$ is even. Because b is even and $h = 1$, r has to be odd and either $b = r - 1$ or $b = r + 1$.
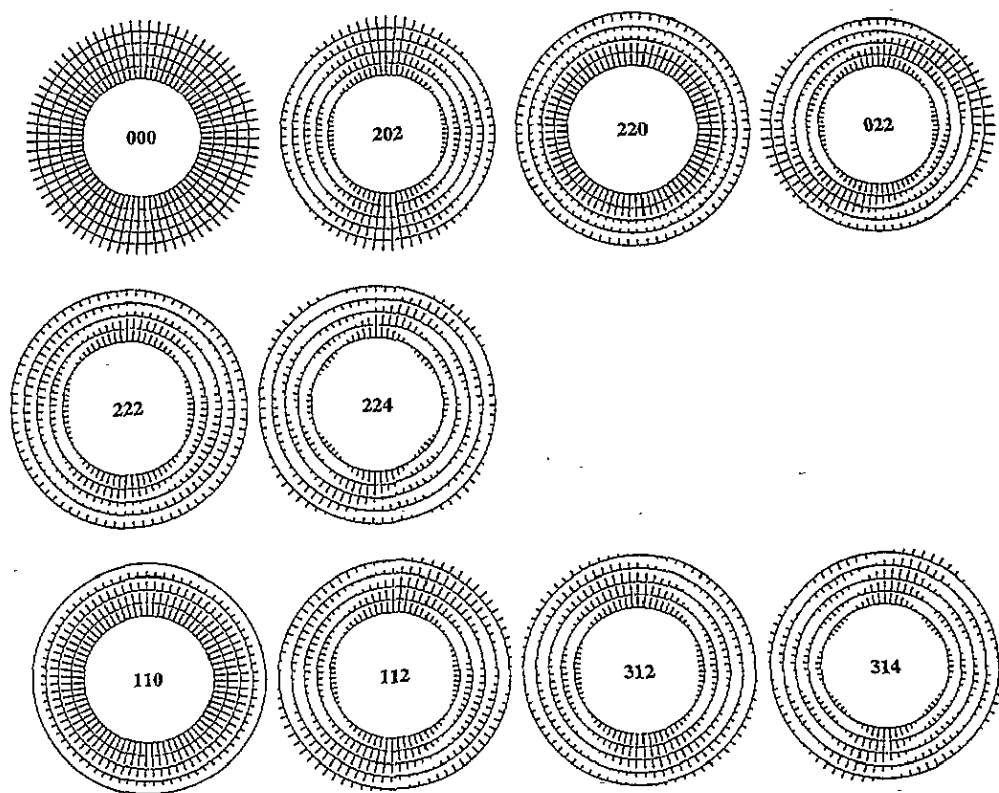
Figure 4. The intensity distributions $U^{zar}(MP\varepsilon) \equiv U^{zar0r}(MPP_S\varepsilon)$ with even r. The values of zar are shown in the middle of each plot. They are the first ten combinations in table 3, needed for spin unpolarized measurements. The plots only show coplanar geometries with M, P and ε in one plane. The magnetization M is along the Z-axis which is vertically upward. The polarization direction P of the light is at an angle θ_P in the XZ plane and the emission direction ε is at θ_ε. The intensity distribution is shown for five values of θ_P, *viz.* $0°$, $22.5°$, $45°$, $67.5°$ and $90°$ corresponding to the five circles, going outward. Each circle has short lines in the radial direction with lengths proportional to the intensity for the corresponding value of θ_ε. So each circle shows the intensity distribution for a fixed value of θ_P. The line at the top of the inner circle has length $U^{zab}(MMM)$ which is unity (for $z + a + r$ even, which is the case for resonant photoemission).

Because $z+a+r$ is even $z+a+h+b$ is even. Therefore, according to rule 3 in appendix B, U will be non-zero in general when all vectors are in the same plane. We will assume that in this case *all* relevant properties of U can be observed in coplanar geometries. From inspection of plots of the complete behaviour of these functions this appears to be certainly true for $z = 0$ and $z = 1$ where, if we take ε and P_S out of the plane of M and P the intensity varies in a very predictable way. For higher z the behaviour becomes more complex, but for simplicity we will here only consider coplanar geometries. The most important fact here is that when M, P and ε are coplanar the polarization vector of P_S (defined formally in appendix B) is also in the plane, because if P_S were perpendicular to it the signal would be zero because $z + a + b$ is odd (rule 1 in appendix B). Due to these simplifications we are able to plot these angle dependences and study many of their features. Figure 5 gives the plots needed for linearly polarized light, $a = 0$ and 2, and figure 6 those for circular polarization, $a = 1$. We see that the polarization can be perpendicular to ε,
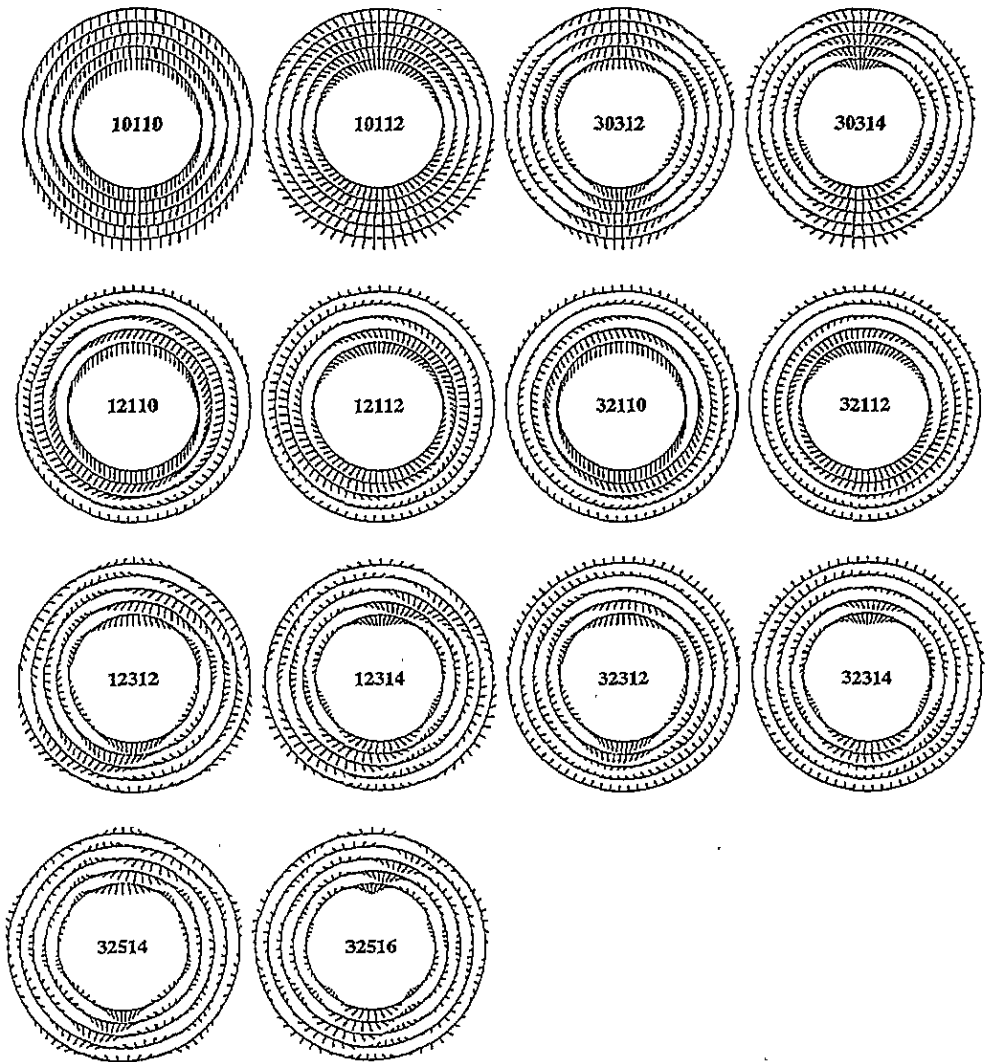
Figure 5. The spin polarization distributions U^{zar1b} for linearly polarized light, $a = 0$ and 2, and for r odd and b even. These distributions are needed for J^{01} and J^{21} in table 3. The plots are essentially the same as figure 4 but now each line gives both magnitude and direction of the spin polarization vector Q. A line pointing outward means polarization along ε. The intensity $U^{zar1b}(MPP_S\varepsilon)$ of the signal obtained with a given spin detection direction P_S is the inner product $P_S \cdot Q$. The values of $zar1b$ are shown in the middle of each plot.

but it is always in the plane. It is striking that the functions appear in strongly resembling pairs $zar1b$ with $b = r - 1$ and $b = r + 1$. This is due to the fact that they have the radial component of the spin polarization the same and that the transverse component has opposite sign, so if in a geometry the distribution with $b = r - 1$ points, say, to the left of the radial direction $b = r + 1$ points to the right. The magnitudes of the transverse components for $b = r + 1$ and $b = r - 1$ can be shown to be related as $-r/(r + 1)$. A consequence is that both distributions have the same geometries in which the spin polarizations are purely radial or purely transverse and antiparallel. Because in (37) the signal is always a sum over two
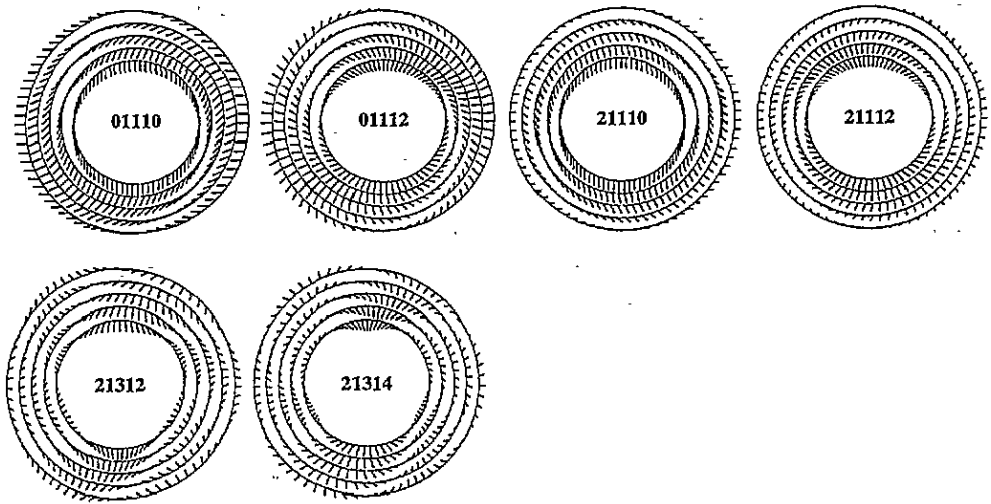
Figure 6. The spin polarization distributions U^{zar1b} for circularly polarized light, $a = 1$ (cf figure 5). These distributions are needed for J^{11} in table 3.

values of b with coefficients B^{r1b}, we do not actually have two distributions but only one, if we consider the ratio of the two to be fixed by the values of the Coulomb radial integrals. The composite distribution does however depend on the final LS state being studied. The overall pattern of geometries with transverse and radial polarization is determined by zar. Actually for the radial component of the polarization, which is measured when P_S is along ε, we have generally, using (B4), $U^{zar1b}(MP\varepsilon\varepsilon) = U^{zar}(MP\varepsilon)$, independent of b. So, we may say that in resonant photoemission we have to measure distributions $U^{zar}(MP\varepsilon)$ for both even and odd r. For even r we detect the total intensity; for odd r we detect the radial component of the spin polarization. Although we do not show U^{zar} for odd r, the features of these functions can be easily deduced from those of U^{zar1b}.

6.3.3. Spin polarization: odd functions. The case when $r+h+b$ is odd is similar. Note that due to the fact that b must be even b can only be equal to r and so r is also even. Further, P_S is polarized perpendicularly to ε because the geometry $P_S\|\varepsilon$ is forbidden by rule 6 in appendix B. It seems that again a geometry with M, P and ε coplanar may be sufficient. In this case P_S is always perpendicular to the plane and the signal is thus automatically separate from signals with $b + h + r$ even. Again the distributions $U^{zar1r}(MPP_S\varepsilon)$ and $U^{zar}(MP\varepsilon)$ are strongly connected.

$$U^{zar1r}(MPP_S\varepsilon) = (-)^{r+1}\frac{2}{2r+1}\frac{\mathrm{d}}{\mathrm{d}\varphi}U^{zar}(MP\varepsilon) \qquad (52)$$

where φ denotes a rotation of ε around P_S. So the derivative gives the change in intensity when ε is rotated around P_S keeping M and P fixed. When P_S is parallel to ε the derivative in (52) is of course zero which gives us another way to see that the polarization cannot be along ε. In figure 7 the perpendicular spin polarization is plotted as the length of a line in the radial direction. We see indeed that each circle for $zar1r$ is the derivative of the corresponding circle in figure 4 for zar. Effectively we have therefore an alternative way to detect a given zar with even r: in addition to measuring the total intensity we may measure the spin polarization perpendicular to the plane and obtain essentially the same information. Because for a p intermediate core hole the only possibility for this is $bhr = 212$, there being

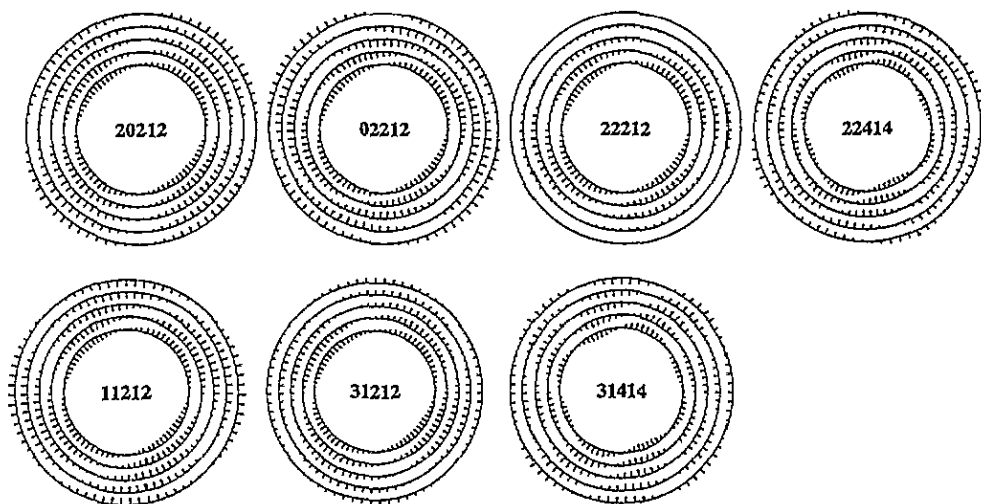no such possibility as 010, the analysis of the signal is simpler than for the total intensity measurement.

Figure 7. The spin polarization distributions U^{zar1r} for even r (cf figures 5 and 6). These distributions are needed for the second group of J^{01}, J^{21} and J^{11} in table 3. In this case the *direction* of the spin polarization is perpendicular to the plane of M, P and ε. Its *magnitude* is plotted as the length of a line in the radial direction. A line pointing outward means that Q is upward out of the paper.

:

There is no indication that in geometries other than coplanar for M, P and ε fundamentally different possibilities are present, but experimentally such geometries may still be interesting, especially with all vectors collinear or perpendicular (cf the examples in appendix B).

6.4. Experimental combinations

6.4.1. Even geometries. We can now given an overview of possible experimental combinations of polarizations. All the possibilities for z up to three are shown in table 3 and the following statements can be easily checked. First, for LS coupled final states we have $b + h + r$ is even. Because b is always even $h + r$ has to be even. This means that even r can only be measured in a spin unresolved measurement ($h = 0$) and that for odd r spin detection is needed ($h = 1$). These signals can be measured in a coplanar geometry, meaning that magnetic moment, light polarization, emission direction and spin detection direction are in one plane, or even in a collinear geometry. In order to measure odd z either the light has to be circularly polarized or the spin of the emitted electron has to be detected.

6.4.2. Odd geometries. If the spin–orbit splitting in the final state is resolved the parity of $h + r$ is no longer restricted. So, with even h we could measure odd r values if not unfortunately the only even value of h available is $h = 0$ which means $r = b$, which is even, so this possibility is excluded. On the other hand it is possible to use $h = 1$ to measure even r. Although even r can already be studied with $h = 0$, the special properties of angular distributions with odd $h + r$ can make the $h = 1$ measurement attractive, e.g. because it may measure exactly one value of r, simplifying the analysis. This would be the

Table 3. Allowed combinations of *zarhb* for *z* up to 3. Considering only $a+z+r =$ even (no axially coupled tensors): if $r+h+b =$ even and $h = 0$ then $r = b =$ even and $a+z =$ even; if $r+h+b =$ even and $h = 1$ then $r =$ odd and $a+z =$ odd; if $r+h+b =$ odd (spin–orbit coupling in final state and interference between continuum channels) then $h = 1$ and $r = b =$ even and $\neq 0$ and $a + z =$ even. This table can be used together with (53) to find all terms in the summations for given *a* and *h* and *z* up to 3. For any application *r* can be limited to $r \leqslant 2j$. The ultimate test for the presence of a term is a non-zero entry for *zar* in table 1 for *C* and for *rhb* in table 4 for β. Table 1 for *C* automatically gives the corresponding values of *x* and *y*.

	z	a	r	h	b
$r+h+b =$ even					
	+	+	+	+	+
J^{00}	0	0	0	0	0
	2	0	2	0	2
J^{20}	2	2	0	0	0
	0	2	2	0	2
	2	2	2	0	2
	2	2	4	0	4
	−	−	+	+	+
J^{10}	1	1	0	0	0
	1	1	2	0	2
	3	1	2	0	2
	3	1	4	0	4
	−	+	−	−	+
J^{01}	1	0	1	1	0
	1	0	1	1	2
	3	0	3	1	2
	3	0	3	1	4
J^{21}	1	2	1	1	0
	1	2	1	1	2
	3	2	1	1	0
	3	2	1	1	2
	1	2	3	1	2
	1	2	3	1	4
	3	2	3	1	2
	3	2	3	1	4
	3	2	5	1	4
	3	2	5	1	6
	+	−	−	−	+
J^{11}	0	1	1	1	0
	0	1	1	1	2
	2	1	1	1	0
	2	1	1	1	2
	2	1	3	1	2
	2	1	3	1	4
$r+h+b =$ odd					
	+	+	+	−	+
J^{01}	2	0	2	1	2
J^{21}	0	2	2	1	2
	2	2	2	1	2
	2	2	4	1	4
	−	−	+	−	+
J^{11}	1	1	2	1	2
	3	1	2	1	2
	3	1	4	1	4

case of a ppp decay with different p levels for the final state core holes. Here the $^3D_{1,2,3}$ states, which only give an 'odd' signal for $bhr = 212$ (the only possibility here because $r = 4$ cannot be reached in a p core hole), would allow pure measurement of $r = 2$. If we choose P, M and ε to be coplanar and take P_S perpendicular to the plane we measure $r = 2$ with still freedom to vary P, M and ε. So it would seem that use of spin–orbit split final states in order to measure with odd $h + r$ can be useful for our purpose as a probe of the ground state. Moreover it is still useful as a method to obtain knowledge on the final states, which is ultimately needed for their use as a probe.

7. Application

7.1. Decay following $p \to d$ absorption

As an illustration for the use of the theory we consider here the decay of a 2p core hole to a two-core-hole state in a 3d transition metal. We want to know the intensities J^{ah} for the spin integrated ($h = 0$) and spin polarized ($h = 1$) photoemission using isotropic light ($a = 0$), circular dichroism ($a = 1$) and linear dichroism ($a = 2$).

In cylindrical symmetry (37) can be written as

$$4\pi J_j^{ah}(LS; MPP_S\varepsilon) = \sum_{zrb} \left\{ \sum_{xy} \langle \underline{w}^{xyz}\rangle C_j^{xyzar} \right\} U^{zarhb}(MPP_S\varepsilon) B_j^{rhb}(LS) \tag{53}$$

where we must fill in the values of the moments allowed by the triangle conditions, of which the most important ones are summarized in figure 8. For convenience the allowed combinations of $zarhb$ are given in table 3. The next most important condition is $r \leqslant 2j$. So we have for the $j = \frac{1}{2}$ edge only $r = 0$ and 1. For example, for $ah = 10$ we find from table 3 the entry $zarhb = 11\,000$ and then for $zar = 110$ we find $\sum_{xy} C_j^{xyzar} \underline{w}^{xyz}$ from table 1. The result is

$$4\pi J_{1/2}^{00} = (\underline{w}^{000} - \underline{w}^{110}) U^{00000} B_{1/2}^{000} \tag{54}$$

$$4\pi J_{1/2}^{10} = \tfrac{1}{3}(-\underline{w}^{011} + 3\underline{w}^{101} - 2\underline{w}^{211}) U^{11000} B_{1/2}^{000} \tag{55}$$

$$4\pi J_{1/2}^{20} = \tfrac{1}{5}(-2\underline{w}^{112} + 5\underline{w}^{202} - 3\underline{w}^{312}) U^{22000} B_{1/2}^{000}. \tag{56}$$

For the $j = \frac{3}{2}$ edge $r \leqslant 3$ so that

$$4\pi J_{3/2}^{00} = (2\underline{w}^{000} + \underline{w}^{110}) U^{00000} B_{3/2}^{000} + (2\underline{w}^{112} + \underline{w}^{202}) U^{20202} B_{3/2}^{202} \tag{57}$$

$$\begin{aligned}4\pi J_{3/2}^{10} &= \tfrac{1}{3}(\underline{w}^{011} + 6\underline{w}^{101} + 2\underline{w}^{211}) U^{11000} B_{3/2}^{000} + \tfrac{2}{15}(5\underline{w}^{011} + 3\underline{w}^{101} + \underline{w}^{211}) U^{11202} B_{3/2}^{202} \\ &\quad + \tfrac{3}{5}(2\underline{w}^{213} + \underline{w}^{303}) U^{31202} B_{3/2}^{202}\end{aligned} \tag{58}$$

$$\begin{aligned}4\pi J_{3/2}^{20} &= \tfrac{1}{5}(2\underline{w}^{112} + 10\underline{w}^{202} + 3\underline{w}^{312}) U^{22000} B_{3/2}^{000} + \tfrac{1}{5}(\underline{w}^{000} + 2\underline{w}^{110}) U^{02202} B_{3/2}^{202} \\ &\quad + \tfrac{2}{35}(7\underline{w}^{112} + 5\underline{w}^{202} + 3\underline{w}^{312}) U^{22202} B_{3/2}^{202}.\end{aligned} \tag{59}$$

For the U functions we use

$$U^{zar0r}(MPP_S\varepsilon) = U^{zar}(MP\varepsilon). \tag{60}$$

Some $U^{zar}(MP\varepsilon)$ are given in table 1 of [71] in the form $U^{arz}(P\varepsilon M)$; we add here U^{312}, and find for the U functions in the circular dichroism

$$U^{11000} = M \cdot P \tag{61}$$

$$U^{11202} = -\tfrac{1}{2}M \cdot P + \tfrac{3}{2}(M \cdot \varepsilon)(\varepsilon \cdot P) \tag{62}$$

$$U^{31202} = -\tfrac{1}{2}M \cdot P - (M \cdot \varepsilon)(\varepsilon \cdot P) + \tfrac{5}{2}(M \cdot P)(\varepsilon \cdot M)^2. \tag{63}$$

These functions are plotted in figure 4. It is natural that $J_{1/2}^{10}$ has a $P \cdot M$ dependence exactly as the XAS signal, since for $r = 0$ the core hole is not polarized. The angular dependence of $J_{3/2}^{10}$ is more interesting and by changing angles between P, ε and M we obtain different values from the U functions so that in principle we can separate the three different linear combinations of $\underline{w}^{xyz}$. For $P \cdot M = 0$ the terms in $J_{3/2}^{10}$ containing B^{000} are zero.
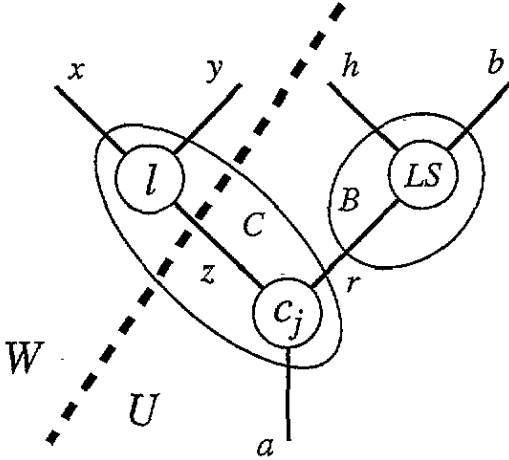
Figure 8. A schematic picture to illustrate the most important triangle conditions in (53) for the multipole moment W, the angle dependent function U, the excitation strength C and the decay strength B.

The U functions in the isotropic spectrum and linear dichroism are

$$U^{00000} = 1 \tag{64}$$

$$U^{02202} = \tfrac{3}{2}(P \cdot \varepsilon)^2 - \tfrac{1}{2} \tag{65}$$

$$U^{20202} = \tfrac{3}{2}(\varepsilon \cdot M)^2 - \tfrac{1}{2} \tag{66}$$

$$U^{22000} = \tfrac{3}{2}(M \cdot P)^2 - \tfrac{1}{2} \tag{67}$$

$$U^{22202} = 1 - \tfrac{3}{2}(\varepsilon \cdot M)^2 - \tfrac{3}{2}(M \cdot P)^2 - \tfrac{3}{2}(P \cdot \varepsilon)^2 + \tfrac{9}{2}(P \cdot \varepsilon)(\varepsilon \cdot M)(M \cdot P). \tag{68}$$

To remove the dependence on B^{000} one should measure under the magic angle, where $M \cdot P = \tfrac{1}{3}\sqrt{3}$.

7.2. Decay strength in LS coupling

(54)–(59) are valid for decay processes following p $\rightarrow$ d excitation, where the final state dependence is contained in B. For further evaluation the expression for B is decomposed in a manner already apparent from (39).

$$B_j^{rhb}(LS) = \tau \sum_{e\underline{e}} \beta_j^{rhb}(LSe\underline{e})R(LSe)R(LS\underline{e})e^{i(\delta_e - \delta_{\underline{e}})} \tag{69}$$

with

$$R(LSe) = \sum_k r^k R_{cpde}^k + e^k E_{cpde}^k \tag{70}$$

$$E_{cpde}^k \equiv R_{cdpe}^k. \tag{71}$$

Table 4. The non-zero coefficients $\beta_{3/2}^{rhb}(LS\underline{e}e)$ for LS final states in a ppp process. The values for rhb are indicated at the top of each column. Note that the values for singlet and triplet differ by a factor of 3 for $h = 0$ and -1 for $h = 1$. The values for $e\underline{e} = $ pf and fp are equal, together producing a phase shift factor in (39) of $2\cos(\delta_p - \delta_f)$. The corresponding $R(LS e)$ are in table 5.

LS	$e\underline{e}$	000	110	112	202	312
^{3}D	pp	5/2	−5/6	1/30	−1/4	1/20
	pf			9/125	−27/50	27/250
	ff	27/125	−9/125	36/3125	−54/625	54/3125
^{3}P	pp	3/2	−1/2	−1/10	3/4	−3/20
^{3}S	pp	1/2	−1/6	1/15	−1/2	1/10
^{1}D	pp	5/6	5/6	−1/30	−1/12	−1/20
	pf			−9/125	−9/50	−27/250
	ff	9/125	9/125	−36/3125	−18/625	−54/3125
^{1}P	pp	1/2	1/2	1/10	1/4	3/20
^{1}S	pp	1/6	1/6	−1/15	−1/6	−1/10

$\tau = 1$ for final state holes in different shells and $1/2$ for final state holes in the same shell. The possible values of k in R_{cpde}^k are

$$k = \max(|c - d|, |p - e|), \ldots, \min(c + d, p + e) \text{ step } 2 \tag{72}$$

where $c + d$ and $p + e$ must be both even or both odd. For k in E_{cpde}^k we have (72) with p and d interchanged.

As an example we will evaluate the B values for the p$_{3/2}$pp decay. The values of β for this decay are given in table 4. The expressions for $R(LS e)$ are in table 5. Together they contain the expressions for the B for $j = \frac{3}{2}$ for a p$_{3/2}$pp process in terms of the radial integrals R. From table 4 we see

$$B_{3/2}^{000}(^3P) = \tfrac{3}{2}R(^3Pp)^2 \tag{73}$$

$$B_{3/2}^{202}(^3P) = \tfrac{3}{4}R(^3Pp)^2 \tag{74}$$

$$B_{3/2}^{000}(^1D) = \tfrac{5}{6}(^1Dd)^2 + \tfrac{9}{125}R(^1Df)^2 \tag{75}$$

$$B_{3/2}^{202}(^1D) = -\tfrac{1}{12}R(^1Dp)^2 - \tfrac{9}{25}R(^1Dp)R(^1Df)\cos(\delta_f - \delta_p) - \tfrac{18}{625}R(^1Df)^2 \tag{76}$$

$$B_{3/2}^{000}(^1S) = \tfrac{1}{6}R(^1Sp)^2 \tag{77}$$

$$B_{3/2}^{202}(^1S) = -\tfrac{1}{6}R(^1Sp)^2. \tag{78}$$

Using from table 5

$$R(^3Pp) = R_p^0 + E_p^0 - \tfrac{1}{5}R_p^2 - \tfrac{1}{5}E_p^2 \tag{79}$$

$$R(^1Dp) = R_p^0 + E_p^0 + \tfrac{1}{25}R_p^2 + \tfrac{1}{25}E_p^2 \tag{80}$$

$$R(^1Df) = R_f^2 + E_f^2 \tag{81}$$

$$R(^1Sp) = R_p^0 + E_p^0 + \tfrac{2}{5}R_p^2 + \tfrac{2}{5}E_p^2 \tag{82}$$

with the Hartree–Fock values [56] $R_p^0 = 0.070\,19$ eV$^{1/2}$, $R_p^2 = 0.045\,24$ eV$^{1/2}$, $R_f^2 = 0.080\,03$ eV$^{1/2}$, $\delta_f - \delta_p = 2.45$ rad, and for two holes in the same shell $E_e^k = R_e^k$ and $\tau = \frac{1}{2}$ we obtain for $B(\times 10^4)$

$$B_{3/2}^{000}(^3P) = 112.15 \qquad B_{3/2}^{202}(^3P) = 56.08 \tag{83}$$

$$B_{3/2}^{000}(^1D) = 95.62 \qquad B_{3/2}^{202}(^1D) = 19.53 \tag{84}$$

Table 5. $R(LSe)$ expanded into $R^k(cpde)$ and $E^k(cpde) = R^k(cdpe)$ for $cdp = ppp$. R^k_e is shorthand for $R^k(pppe)$. When p and d (i.e. the final two p shells in this case) are equivalent electrons only terms with $L + S$ even have to be considered, the E integrals should be omitted and afterward the total intensity has to be multiplied by two. Alternatively R and E may simply be substituted after which the total intensity has to be multiplied by $\tau = \frac{1}{2}$, and, because for equivalent electrons $R^k = E^k$, states with odd $L + S$ have zero intensity. Note that the entries for singlet and triplet are equal for R integrals and have opposite sign for E integrals. Further R^k and E^k have the same coefficient when $L + S$ is even and opposite sign when $L + S$ is odd.

LS	e	R^0_p	E^0_p	R^2_p	E^2_p	R^2_f	E^2_f
^3D	p	1	-1	1/25	$-1/25$		
	f					1	-1
^3P	p	1	1	$-1/5$	$-1/5$		
^3S	p	1	-1	2/5	$-2/5$		
^1D	p	1	1	1/25	1/25		
	f					1	1
^1P	p	1	-1	$-1/5$	1/5		
^1S	p	1	1	2/5	2/5		

$$B^{000}_{3/2}(^1S) = 25.98 \qquad B^{202}_{3/2}(^1S) = -25.98. \tag{85}$$

Since $E^k_e = R^k_e$ we see immediately from table 5 that $B^{zhb} = 0$ for the Pauli forbidden states ^3D, ^3S and ^1P.

As is apparent from (73), (74), (77) and (78) for ^1S and ^3P the ratios B^{202}/B^{000} are fixed numbers, independent of the value of the radial integrals. In fact the ratios of all B values can be found using only a single row of table 4. As discussed in section 5 this situation occurs for states that can be reached in only one continuum channel. ^1D can be reached in the p and f channels and so the radial integrals and phase difference are important.

7.3. Spin detection

For $r + h + b$ is even we obtain

$$4\pi J^{01}_{3/2} = \tfrac{1}{9}(10\underline{w}^{011} + 15\underline{w}^{101} + 2\underline{w}^{211})(U^{10110}B^{110}_{3/2} + U^{10112}B^{112}_{3/2}) + 3\underline{w}^{213}U^{30312}B^{312}_{3/2} \tag{86}$$

$$4\pi J^{11}_{3/2} = \tfrac{1}{9}(5\underline{w}^{000} + 4\underline{w}^{110})(U^{01110}B^{110}_{3/2} + U^{01112}B^{112}_{3/2})$$
$$+\tfrac{2}{45}(17\underline{w}^{112} + 25\underline{w}^{202} + 3\underline{w}^{312})(U^{21110}B^{110}_{3/2} + U^{21112}B^{112}_{3/2})$$
$$+\tfrac{3}{35}(14\underline{w}^{112} + \underline{w}^{312})(U^{21312}B^{312}_{3/2}) \tag{87}$$

$$4\pi J^{21}_{3/2} = \tfrac{2}{45}(\underline{w}^{011} + 15\underline{w}^{101} + 22\underline{w}^{211})(U^{12110}B^{110}_{3/2} + U^{12112}B^{112}_{3/2})$$
$$+\tfrac{1}{35}(24\underline{w}^{213} + 35\underline{w}^{303} + 4\underline{w}^{413})(U^{32110}B^{110}_{3/2} + U^{32112}B^{112}_{3/2})$$
$$+\tfrac{2}{35}(7\underline{w}^{011} + 2\underline{w}^{211})U^{12312}B^{312}_{3/2} + \tfrac{4}{35}(6\underline{w}^{213} + \underline{w}^{413})U^{32312}B^{312}_{3/2} \tag{88}$$

where we used from table 4 that $B^{314} = 0$. The U functions are plotted in figures 5 and 6.

7.4. Decay strength in LSJ coupling

For LSJ coupled final states the procedure is quite similar. We use table 6 together with table 5. The sum over all J levels belonging to an LS term gives the LS entry in table 4. For $L = 0$ or $S = 0$ the entries in these tables are therefore the same. The omitted entries in table 4 are zero by straightforward triangular relations that can be read from the formula or from the graphs. The zeros in the 212 column are due to the antisymmetry of (45) or

$r + h$ odd. Non-zero elements can only occur in spin–orbit split LS levels in interference channels and are purely imaginary, giving a phase factor of $-2\sin(\delta_e - \delta_{\underline{e}})$. The zeros in the 314 column are due to the fact that $b = 4$ can only be reached in the presence of spin–orbit coupling in the final states. Therefore 314 is zero for $L = 0$ or $S = 0$ states. The zeros in other columns are accidental.

Table 6. $\beta^{rhb}(LSJe\underline{e})$. Rows with $e \neq \underline{e}$ have been given only for $\underline{e} > e$. The row with $\underline{e} < e$ is the complex conjugate. This means that for a real entry for $e \neq \underline{e}$ ($r + h$ even) the phase factor in (42) gives $2\cos(\delta_e - \delta_{\underline{e}})$ and for an imaginary entry ($r + h$ odd) it is $-2\sin(\delta_e - \delta_{\underline{e}})$ which includes the i factor in the table entry. The corresponding $R(LSe)$ are in table 5.

LSJ	$e\underline{e}$	000	110	112	202	212	312	314
$^3D_1$	pp	1/8	11/120	17/150	1/10	0	1/50	
	pf		−27/625	−27/500		3i/40	171/17 500	−18/875
	ff	81/1250	−243/6250	972/15 625	−162/3125	0	486/109 375	−324/21 875
$^3D_2$	pp	5/8	1/8	−1/2·	0	0	0	
	pf		0		−3/20	i/8	39/700	6/175
	ff	21/250	−39/1250	−12/625	−6/125	0	18/4375	108/4375
$^3D_3$	pp	7/4	−21/20	21/50	−7/20	0	3/100	
	pf			72/625	−42/125	−i/5	186/4375	−12/875
	ff	42/625	−6/3125	−492/15 625	42/3125	0	954/109 375	−216/21 875
$^3P_0$	pp	1/12	1/12	−1/30	−1/12	0	−1/20	
$^3P_1$	pp	3/8	−1/8	1/2	0	0	0	
$^3P_2$	pp	25/24	−11/24	−17/30	5/6	0	−1/10	
$^3S_1$	pp	1/2	−1/6	1/15	−1/2	0	1/10	
$^1D_2$	pp	5/6	5/6	−1/30	−1/12	0	−1/20	
	pf			−9/125	−9/50	0	−27/250	0
	ff	9/125	9/125	−36/3125	−18/625	0	−54/3125	0
$^1P_1$	pp	1/2	1/2	1/10	1/4	0	3/20	
$^1S_0$	pp	1/6	1/6	−1/15	−1/6	0	−1/10	

For $r + h + b$ is odd the intensities are

$$4\pi J^{01}_{3/2} = (2\underline{w}^{112} + \underline{w}^{202})U^{20212}B^{212}_{3/2} \tag{89}$$

$$4\pi J^{11}_{3/2} = \tfrac{2}{15}(5\underline{w}^{011} + 3\underline{w}^{101} + \underline{w}^{211})U^{11212}B^{212}_{3/2}$$
$$+ \tfrac{1}{35}(24\underline{w}^{213} + 35\underline{w}^{303} + 4\underline{w}^{413})U^{31212}B^{212}_{3/2} \tag{90}$$

$$4\pi J^{21}_{3/2} = \tfrac{1}{5}(\underline{w}^{000} + 2\underline{w}^{110})U^{02212}B^{212}_{3/2} + \tfrac{2}{35}(7\underline{w}^{112} + 5\underline{w}^{202} + 3\underline{w}^{312})U^{22212}B^{212}_{3/2}. \tag{91}$$

For the decay to a p^4 final state $B^{212} = 0$, but for a final state with holes in two different p shells $B^{212}(^3D)$ is proportional to $R(^3Dp)R(^3Df)\sin(\delta_f - \delta_p)$. The U functions are plotted in figure 7.

7.5. Decay strength in jjJ coupling

For completeness we have also tabulated the case of jjJ coupling for the final states. The separation of terms in jjJ coupling is less complete than in LS coupling, which makes the use of the formulae a little more tedious. Tables 7 and 8 can however be used in much the same way, only more rows have to be added for each state. The separation into two tables is possible according to the following formula:

$$B^{rhb}_j(j_p j_d J) = \sum_{ej\underline{e}j_{\underline{e}}} \beta^{rhb}_j(j_p j_d Jej\underline{e}j_{\underline{e}})R(j_p j_d Jej)R(j_p j_d J\underline{e}j_{\underline{e}})e^{i(\delta_e - \delta_{\underline{e}})}. \tag{92}$$

For $r + h + b$ odd, terms with $e = \underline{e}$ but $j_e \neq j_{\underline{e}}$ have a zero phase factor because $\delta_e - \delta_{\underline{e}}$ is zero. So these terms do not have to be considered. They will only contribute if the phase shift depends on j_e.

7.6. B^{zhb} spectra

For comparison with measurements it is most useful to plot the B^{zhb} spectra of the different decay channels. We will do this here for the decay from the $2p_{3/2}$ level in Ni d^9, since for the intermediate state p^5d^{10} we can also evaluate the B spectra of the psd, ppd and pdd decays, similarly as for the ppp decay.

The B spectra of the ppp decay are shown in figure 9. As a slight complication the $3p^4$ final state has a strong intra-atomic configuration interaction (CI) with the $3s^1d^9$ final state, which is split into a ^1D and a ^3D state. The β values and R integrals for the psd decay are given in tables 9 and 10, respectively. The CI has a large matrix element $R^1(3p, 3p; 3s, 3d)$ which pushes the ^1D peak of the $3s^1d^9$ structure toward the ^3D peak and the ^1D of the $3p^4$ structure toward the ^1S peak. This means that the spectra for the ppp decay are essentially split in a $^1S + {}^1D$ peak and a ^3P peak. The CI mixes the two ^1D states by 17%, so that intensity is transferred between the two states. We estimate the order of magnitude of this effect by assuming that the B values of the states can be obtained by taking the sum over the pure states weighted by the mixing coefficients. In the isotropic spectrum the $3s^1d^9$ gains intensity. The ^1D to ^3D separation in the psd structure is no longer a good measure for the exchange interaction. In fact, the experimentally observed peak splitting of ~ 6 eV [24] is due to the separation of the $3s^1d^9$ and $3s^1d^{10}$ configurations. For simplicity we have omitted the $3s^1d^{10}$ configuration, which is only accessible by direct photoemission from the d^{10} configuration in the initial state and not by resonant photoemission.

The isotropic spectrum B^{000} shows a triplet and a singlet peak with comparable intensities in agreement with experimental results and previous calculations [24, 25]. The B^{110} spectrum gives the angle integrated spin spectrum. Singlet states and triplet states have spin polarizations ($= B^{110}/B^{000}$) of unity and $-1/3$, respectively (cf table 4). The spectra with $b \neq 0$ can only be observed in the angle dependence and they will vanish in the angle integrated emission. In LS coupling the B^{312} spectrum is equal to the B^{112} spectrum multiplied by 3/2. Thus in this coupling the angle dependence (i.e. $b = 2$) can be fully described by a spin integrated spectrum B^{202} and a spin difference spectrum $B^{112} + B^{312}$ or, if preferred, a spin-up and a spin-down spectrum.

Spin–orbit coupling in the final state splits the ^3P peak. This peak will display additional fine structure in the B^{110} and B^{202} spectra as is clear from table 6 for LSJ coupling which shows opposite signs for the $^3P_2$ and $^3P_0$ levels. Spin–orbit coupling also introduces a difference between the B^{112} and B^{312} spectra. However, for the 3d metals the 3p spin–orbit coupling is small compared to the 3p–3p electrostatic interactions, so that the sum over the J levels, i.e. the LS coupling result, is a reasonable approximation.

In [37] the circular dichroism in the Ni ppp decay was measured for a geometry with $P \cdot M = 0$, so that the B^{000} contribution vanishes. The J^{10} value is then proportional to $B^{202}_{3/2}$ which according to (83)–(85) gives $^3P : ({}^1D + {}^1S) = 1 : (-0.12)$. With CI this ratio changes to $1 : (-0.19)$. However, the experiment showed a smaller triplet peak but a larger singlet peak than the theory. In [37] this was accommodated by using the phase difference to fit the experiment. For $\delta_f - \delta_p = 1.1$ rad $B^{202}_{3/2}({}^1D)$ in (84) changes from 19.53 to -18.8, so that the J^{10} signal of $^1D + {}^1S$ gives about the same value as the ^3P signal with opposite sign. However, there seems to be no reason to assume that the Hartree–Fock value is so much in error because atomic calculations with different numbers of electrons,

Table 7. Coefficients $\beta^{rhb}(j_p j_d J e j_e \underline{e}\underline{j_c})$ in (92) for jjJ coupled final states of a ppp process. Rows with $e j_e \neq \underline{e}\underline{j_c}$ have been given only once; the row with $e j_e$ and $\underline{e}\underline{j_c}$ interchanged is the complex conjugate. This means that for a real entry for $e j_e \neq \underline{e}\underline{j_c}$ ($r+h$ even) the phase factor in (42) gives $2\cos(\delta_e - \delta_{\underline{e}})$ and for an imaginary entry ($r+h$ odd) it is $-2\sin(\delta_e - \delta_{\underline{e}})$ which includes the i factor in the table entry. The table entries for $(\frac{3}{2}\frac{1}{2})J$ and $(\frac{1}{2}\frac{3}{2})J$ are equal. Therefore only $(\frac{1}{2}\frac{3}{2})J$ is given. The final expressions for the intensities of $(\frac{3}{2}\frac{1}{2})J$ and $(\frac{1}{2}\frac{3}{2})J$ are the same except that R and E integrals are interchanged. The $R(j_p j_d J e j_e)$ corresponding to this table are in table 8.

$j_p j_d J e j_e \underline{e}\underline{j_c}$	000	110	112	202	212	312	314
$\frac{1}{2}\frac{1}{2}0\,p\frac{3}{2}p\frac{3}{2}$	1/50	1/50	−1/125	−1/50	0	−3/250	
$\frac{1}{2}\frac{1}{2}1\,p\frac{3}{2}p\frac{3}{2}$	3/250	11/1250	−11/3125	−3/1250	0	27/6250	
$p\frac{3}{2}f\frac{5}{2}$			−54/3125	−6/625	i/50	48/21875	24/4375
$f\frac{5}{2}f\frac{5}{2}$	6/125	−18/625	144/3125	−24/625	0	72/21875	−48/4375
$\frac{1}{2}\frac{3}{2}1\,p\frac{1}{2}p\frac{1}{2}$	3/4	−1/4	1				
$p\frac{1}{2}p\frac{3}{2}$		−2/25	−1/25	−3/25	−3i/20		
$p\frac{1}{2}f\frac{5}{2}$				−3/100	i/40	3/700	−6/175
$p\frac{3}{2}p\frac{3}{2}$	3/125	11/625	−22/3125	−3/625	0	27/3125	
$p\frac{3}{2}f\frac{5}{2}$			27/3125	3/625	−i/100	−24/21875	−12/4375
$f\frac{5}{2}f\frac{5}{2}$	3/500	−9/2500	18/3125	−3/625	0	9/21875	−6/4375
$\frac{1}{2}\frac{3}{2}2\,p\frac{1}{2}p\frac{1}{2}$	5/4	1/4	−1				
$p\frac{1}{2}p\frac{3}{2}$		2/25	1/25	−1/25	−i/20		
$p\frac{1}{2}f\frac{5}{2}$				−21/100	7i/40	−3/700	6/175
$p\frac{1}{2}f\frac{7}{2}$						−144/1225	−24/1225
$p\frac{3}{2}p\frac{3}{2}$	1/125	1/625	−2/3125	3/625	0	−3/3125	
$p\frac{3}{2}f\frac{5}{2}$			−63/3125	−3/625	i/100	−24/21875	−12/4375
$p\frac{3}{2}f\frac{7}{2}$				−72/4375	−12i/875	−216/30625	48/30625
$f\frac{5}{2}f\frac{5}{2}$	21/500	−39/2500	78/3125	3/625	0	−81/21875	54/4375
$f\frac{5}{2}f\frac{7}{2}$		144/4375	72/4375	72/4375	6i/125	−288/30625	−216/30625
$f\frac{7}{2}f\frac{7}{2}$	72/875	1944/30625	−1296/30625	−72/1225	0	−2376/214375	864/214375
$\frac{3}{2}\frac{3}{2}0\,p\frac{3}{2}p\frac{3}{2}$	1/4	1/4	−1/10	−1/4	0	−3/20	
$\frac{3}{2}\frac{3}{2}1\,p\frac{1}{2}p\frac{1}{2}$	3/125	−1/125	4/125				
$p\frac{1}{2}p\frac{3}{2}$		−2/25	−1/25	−3/25	−3i/20		
$p\frac{1}{2}f\frac{5}{2}$				3/625	−i/250	−3/4375	24/4375
$p\frac{3}{2}p\frac{3}{2}$	3/4	11/20	−11/50	−3/20	0	27/100	
$p\frac{3}{2}f\frac{5}{2}$			−27/625	−3/125	i/20	24/4375	12/875
$f\frac{5}{2}f\frac{5}{2}$	3/625	−9/3125	72/15625	−12/3125	0	36/109375	−24/21875
$\frac{3}{2}\frac{3}{2}2\,p\frac{1}{2}p\frac{1}{2}$	1/125	1/625	−4/625				
$p\frac{1}{2}p\frac{3}{2}$		2/25	1/25	−1/25	−i/20		
$p\frac{1}{2}f\frac{5}{2}$				−3/625	i/250	−3/30625	24/30625
$p\frac{1}{2}f\frac{7}{2}$						−144/30625	−24/30625
$p\frac{3}{2}p\frac{3}{2}$	5/4	1/4	−1/10	3/4	0	−3/20	
$p\frac{3}{2}f\frac{5}{2}$			−9/125	−3/175	i/28	−24/6125	−12/1225
$p\frac{3}{2}f\frac{7}{2}$				−18/175	−3i/35	−54/1225	12/1225
$f\frac{5}{2}f\frac{5}{2}$	3/875	−39/30625	312/153125	12/30625	0	−324/1071875	216/214375
$f\frac{5}{2}f\frac{7}{2}$		144/30625	72/30625	72/30625	6i/875	−288/214375	−216/214375
$f\frac{7}{2}f\frac{7}{2}$	18/875	486/30625	−324/30625	−18/1225	0	−594/214375	216/214375
$\frac{3}{2}\frac{3}{2}3\,p\frac{3}{2}p\frac{3}{2}$	7/4	−21/20	21/50	−7/20	0	3/100	
$p\frac{3}{2}f\frac{5}{2}$			72/625	−24/875	2i/35	−48/30625	−24/6125
$p\frac{3}{2}f\frac{7}{2}$				−54/175	−9i/35	54/1225	−12/1225
$f\frac{5}{2}f\frac{5}{2}$	24/4375	−24/153125	192/765625	528/153125	0	1296/5359375	−864/1071875
$f\frac{5}{2}f\frac{7}{2}$		−432/30625	−216/30625	−72/30625	−6i/875	−576/214375	−432/214375
$f\frac{7}{2}f\frac{7}{2}$	54/875	162/6125	−108/6125	18/1225	0	594/42875	−216/42875
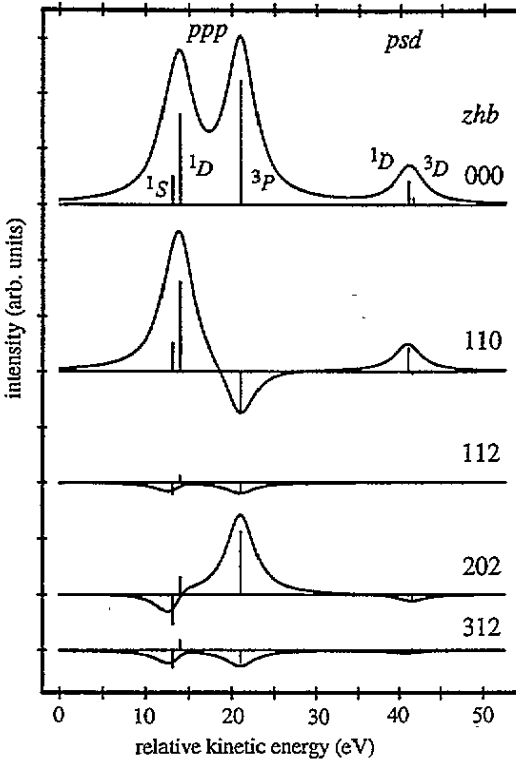
Figure 9. Calculated $B^{zhb}_{3/2}$ spectra for ppp and psd decay in LS coupling for Ni d^9 using Cowan's code [56] with Hartree–Fock values of the Slater integrals $G^2(3s, 3d) = 12.880$ and $F^2(3p, 3p) = 15.911$ eV, which are reduced by $\kappa = 0.8$, and radial matrix elements $R^0(2p, 3p; 3p, \varepsilon_p) = 0.070\,19$, $R^2(2p, 3p; 3p, \varepsilon_p) = 0.045\,24$, $R^2(2p, 3p; 3p, \varepsilon_f) = 0.080\,03$, $R^1(2p, 3s; 3d, \varepsilon_p) = 0.002\,915$, $E^1(2p, 3s; 3d, \varepsilon_p) = -0.035\,00$, $R^1(2p, 3s; 3d, \varepsilon_f) = 0.017\,83$, $E^3(2p, 3s; 3d, \varepsilon_f) = 0.086\,49$ eV$^{1/2}$, $R^1(3p, 3p; 3s, 3d) = 18.801$ eV, $\delta_f - \delta_p = 2.44$ rad, $BE(3p) - BE(3s) = 20.5$ eV. The spectrum is convoluted with $\Gamma = 2$ eV.

or even different core holes, do not change the value of the phase difference by more than a few hundredths [72]. This discrepancy is one of the problems that remains to be solved.

Figure 10 shows the B spectra for the ppd decay. Tables 11 and 12 give the β-values and R-integrals, respectively. The p^5d^9 final state of the ppd decay shows a splitting into a $^1F + {}^1P$ and a $^3D + {}^3P$ peak. Interference terms appear for the F and P final states. Similar observations concerning the B spectra can be made as for the ppp decay. Figure 11 shows the pdd decay. Tables 13 and 14 give the β-values and R-integrals, respectively. Interference terms appear for the ^1G and ^1D final states. The ^1G is the dominant state in the B spectra of the d^8 final state.

8. Conclusions

We have decomposed the resonant photoemission intensity in such a way that it can be interpreted as a process in which first an excitation is made from a core level to the valence shell, leaving behind a polarized core hole. After this the core hole decays into two shallower core holes in a specific state, which can be selected by the energy of the emitted photoelectron. The non-spherical nature of the core hole together with the properties of the

Table 8. $R(j_p j_d J e j_e)$ expanded into $R^k(cpde)$ and $E^k(cpde) = R^k(cdpe)$ for $cdp = ppp$, where R_e^k is shorthand for $R^k(pppe)$. When p and d (i.e. the final two p shells in this case) are equivalent we have $R^k = E^k$ with as in (69) $\tau = 1/2$. For states with $j_p = j_d$ (3/2, 3/2 and 1/2, 1/2) only even J will have intensity. For states with $j_p \neq j_d$ there are no two different states $j_p j_d J$ and $j_d j_p J$ but only one state which is an antisymmetric combination. The intensity for this state will be obtained by adding the intensities of $(\frac{3}{2}\frac{1}{2})J$ and $(\frac{1}{2}\frac{3}{2})J$, which are equal, however, when $R^k = E^k$.

$j_p j_d J e j_e$	R_p^0	E_p^0	R_p^2	E_p^2	R_f^2	E_f^2
$\frac{1}{2}\frac{1}{2}0p\frac{3}{2}$			1	1		
$\frac{1}{2}\frac{1}{2}1p\frac{3}{2}$			1	−1		
$f\frac{5}{2}$					1	−1
$\frac{1}{2}\frac{3}{2}1p\frac{1}{2}$	1			−1/5		
$p\frac{3}{2}$			1	−1		
$f\frac{5}{2}$					1	−1
$\frac{1}{2}\frac{3}{2}2p\frac{1}{2}$	1			−1/25		
$p\frac{3}{2}$			1	1		
$f\frac{5}{2}$					1	−3/7
$f\frac{7}{2}$						1
$\frac{3}{2}\frac{1}{2}1p\frac{1}{2}$		−1	1/5			
$p\frac{3}{2}$			1	−1		
$f\frac{5}{2}$					1	−1
$\frac{3}{2}\frac{1}{2}2p\frac{1}{2}$		1	−1/25			
$p\frac{3}{2}$			1	1		
$f\frac{5}{2}$					−3/7	1
$f\frac{7}{2}$					1	
$\frac{3}{2}\frac{3}{2}0p\frac{3}{2}$	1	1	1/5	1/5		
$\frac{3}{2}\frac{3}{2}1p\frac{1}{2}$			1	−1		
$p\frac{3}{2}$	1	−1	1/25	−1/25		
$f\frac{5}{2}$					1	−1
$\frac{3}{2}\frac{3}{2}2p\frac{1}{2}$			1	1		
$p\frac{3}{2}$	1	1	−3/25	−3/25		
$f\frac{5}{2}$					1	1
$f\frac{7}{2}$					1	1
$\frac{3}{2}\frac{3}{2}3p\frac{3}{2}$	1	−1	1/25	−1/25		
$f\frac{5}{2}$					1	−1
$f\frac{7}{2}$					1	−1

selected final state then cause a specific spatial and spin distribution of the emitted electron.

The basic assumption underlying this type of analysis is that core–valence interactions do not introduce interference between intermediate states which are in the same edge but separated by more than their lifetime width. This is correct in single-particle theory. Therefore, deviations from our results may be useful in the study of the validity of single-particle theory in the presence of core–valence interactions. In metals single-particle theory should be a good approximation. This is corroborated by the fact that the measured 2p absorption spectra of 3d transition metals have narrow $j = \frac{3}{2}$ and $\frac{1}{2}$ peaks, so that in the intermediate state the interactions between the core hole and the valence electrons are small.

Table 9. $\beta_{3/2}^{rhb}(LSe\underline{e})$ for the LS final states in a psd decay (cf the caption to table 4). The corresponding $R(LSe)$ are in table 10.

LS	e$\underline{e}$	000	110	112	202	312
^{3}D	pp	1/3	−1/9	1/225	−1/30	1/150
	pf			1/25	−3/10	3/50
	ff	1/2	−1/6	2/75	−1/5	1/25
^{1}D	pp	1/9	1/9	−1/225	−1/90	−1/150
	fp			−1/25	−1/10	−3/50
	ff	1/6	1/6	−2/75	−1/15	−1/25

Table 10. $R(LSe)$ expanded into $R^k(cpde)$ and $E^k(cdpe)$ for $cdp = psd$ (cf the caption to table 5).

LS	e	R_p^1	E_p^1	R_f^1	E_f^3
^{3}D	p	1	−1		
	f			1	−3/7
^{1}D	p	1	1		
	f			1	3/7

Table 11. $\beta_{3/2}^{rhb}(LSe\underline{e})$ for the LS final states in a ppd decay (cf the caption to table 4). The corresponding $R(LSe)$ are in table 12.

LS	e$\underline{e}$	000	110	112	202	312
^{3}F	dd	7/2	−7/6	1/15	−1/2	1/10
	dg			18/175	−27/35	27/175
	gg	54/175	−18/175	18/1225	−27/245	27/1225
^{3}D	dd	5/2	−5/6	−1/6	5/4	−1/4
^{3}P	ss	1/3	−1/9			
	sd			−1/15	1/2	−1/10
	dd	3/2	−1/2	1/10	−3/4	3/20
^{1}F	dd	7/6	7/6	−1/15	−1/6	−1/10
	dg			−18/175	−9/35	−27/175
	gg	18/175	18/175	−18/1225	−9/245	−27/1225
^{1}D	dd	5/6	5/6	1/6	5/12	1/4
^{1}P	ss	1/9	1/9			
	sd			1/15	1/6	1/10
	dd	1/2	1/2	−1/10	−1/4	−3/20

In localized compounds the 2p absorption lines display a multiplet structure over several electron volts due to the core valence interactions and interference between the decays from different intermediate states can be expected.

The emission can be calculated using tables for the decay probabilities of final states. The angle and spin dependence of the p$_{3/2}$pp decay is contained in five independent spectra (or four, if spin–orbit coupling is neglected). The resonant photoemission spectrum which is measured at an arbitrary angle is a linear combination of these spectra and can therefore show strongly different peak ratios, which up to now may have been ascribed to 'background effects'.

The first experimental results for the circular dichroism in the 2p$_{3/2}$3p3p decay in

Figure 10. Calculated $B^{zhb}_{3/2}$ spectra for ppd decay in LS coupling for Ni d^9 using Cowan's code [56] with Hartree–Fock values of the Slater integrals $F^2(3p, 3d) = 13.632$ eV, $G^1(3p, 3d) = 16.900$ eV, and $G^3(3p, 3d) = 10.227$ eV, which are reduced by $\kappa = 0.8$, and radial matrix elements $R^2(2p, 3p; 3d, \varepsilon_s) = -0.026\,37$, $E^1(2p, 3p; 3d, \varepsilon_s) = -0.067\,26$, $R^0(2p, 3p; 3d, \varepsilon_d) = 0.045\,68$, $R^2(2p, 3p; 3d, \varepsilon_d) = 0.041\,91$, $E^1(2p, 3p; 3d, \varepsilon_d) = 0.097\,28$, $E^3(2p, 3p; 3d, \varepsilon_d) = 0.041\,80$, $R^2(2p, 3p; 3d, \varepsilon_g) = -0.084\,91$, $E^3(2p, 3p; 3d, \varepsilon_g) = -0.010\,42$ eV$^{1/2}$, $\delta_d - \delta_s = 3.046$, $\delta_g - \delta_d = 1.514$ rad. The spectrum is convoluted with $\Gamma = 1$ eV.

Table 12. $R(LSe)$ expanded into $R^k(cpde)$ and $E^k(cdpe)$ for cdp = ppd (cf the caption to table 5).

LS	e	E^1_s	R^2_s	R^0_d	E^1_d	R^2_d	E^3_d	R^2_g	E^3_g
^3F	d			1	$-2/5$	$2/35$	$-3/245$		
	g							1	$-5/7$
^3D	d			1	$1/5$	$-1/5$	$-3/35$		
^3P	s	1	$-3/5$						
	d			1	$-1/15$	$1/5$	$-9/35$		
^1F	d			1	$2/5$	$2/35$	$3/245$		
	g							1	$5/7$
^1D	d			1	$-1/5$	$-1/5$	$3/35$		
^1P	s	-1	$-3/5$						
	d			1	$1/15$	$1/5$	$9/35$		

ferromagnetic nickel and iron [37] show an effect three times smaller than expected in the ^3P final state but a too large effect in the $^1D + {}^1S$ peak. The latter could only be obtained theoretically by assuming a phase shift which strongly deviates from the Hartree–
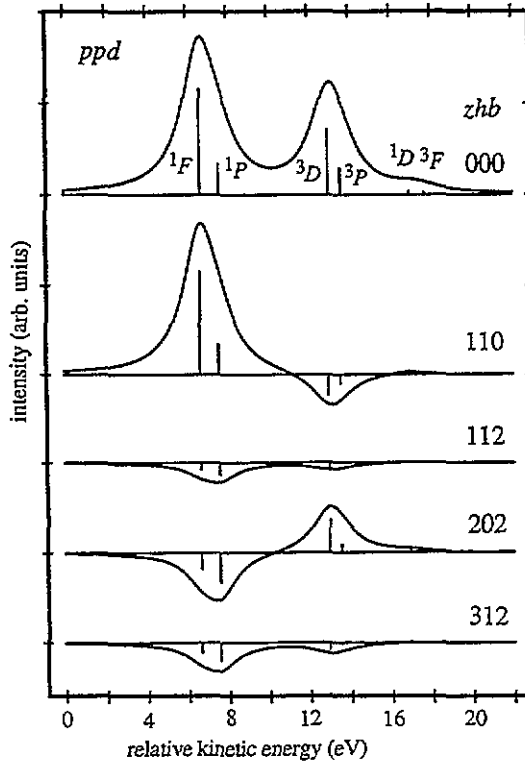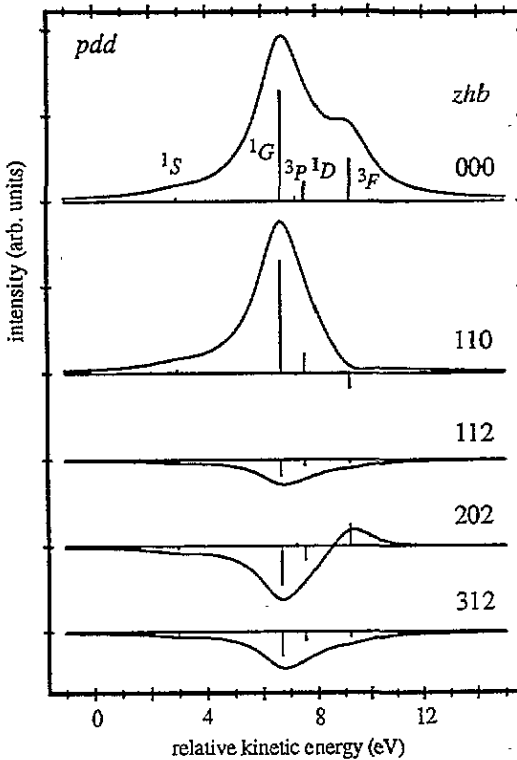
Figure 11. Calculated $B_{3/2}^{zhb}$ spectra for pdd decay in LS coupling for Ni d^9 using Cowan's code [56] with Hartree–Fock values of the Slater integrals $F^2(3d, 3d) = 12.234$ eV and $F^4(3d, 3d) = 7.598$ eV, which are reduced by $\kappa = 0.8$, and radial matrix elements $R^1(2p, 3d; 3d, \varepsilon_p) = -0.048\,92$, $R^3(2p, 3d; 3d, \varepsilon_p) = -0.040\,17$, $R^1(2p, 3d; 3d, \varepsilon_f) = 0.1789$, $R^3(2p, 3d; 3d, \varepsilon_f) = 0.1119$, $R^3(2p, 3d; 3d, \varepsilon_h) = 0.065\,39$ eV$^{1/2}$, $\delta_h - \delta_f = 0.868$, $\delta_f - \delta_p = 2.316$ rad. The spectrum is convoluted with $\Gamma = 1$ eV.

Fock value. These effects need not be entirely due to interference between intermediate states because scattering of the photoelectron and experimental difficulties cannot be ruled out as causes of apparent deviations from the core hole polarization model.

Apart from the quantitative aspects the core hole polarization analysis also has a qualitative value, because at least it allows us to understand the origin and order of magnitude of effects, and suggests suitable experiments to measure them. They can then be calculated afterwards using the full expressions.

From the point of view of the analysis all decay processes into two-core-hole final states contain the same information: they measure the moments of the core hole after absorption. The choice of the best edge for a certain application will depend strongly on the instrumental possibilities. Especially for the very deep core holes, e.g. in the rare earth materials, a diversity of decay processes is available where the two-core-hole states may be in various regimes of Coulomb and spin–orbit coupling. The intensity of the decay and the splitting of the peaks of interest from the rest of the spectrum also determine its value as a probe of core hole polarization.

Measurement of the spin polarization can be useful to find the ground state expectation values of all possible one-electron operators, even though spin–orbit coupling in the initial core hole already allows determination of spin properties from the angle dependence of

Table 13. $\beta_{3/2}^{rhb}(LSee)$ for the LS final states in a pdd decay (cf the caption to table 4). The corresponding $R(LSe)$ are in table 14.

LS	ee	000	110	112	202	312
^3G	ff	27/35	−9/35	3/175	−9/70	9/350
	fh			2/49	−15/49	3/49
	hh	75/343	−25/343	10/1029	−25/343	5/343
^3F	ff	1/5	−1/15	−1/75	1/10	−1/50
^3D	pp	7/30	−7/90	7/2250	−7/300	7/1500
	pf			12/875	−18/175	18/875
	ff	144/1715	−48/1715	192/42 875	−288/8575	288/42 875
^3P	pp	3/10	−1/10	−1/50	3/20	−3/100
^3S	pp	2/15	−2/45	4/225	−2/15	2/75
^1G	ff	9/35	9/35	−3/175	−3/70	−9/350
	fh			−2/49	−5/49	−3/49
	hh	25/343	25/343	−10/1029	−25/1029	−5/343
^1F	ff	1/15	1/15	1/75	1/30	1/50
^1D	pp	7/90	7/90	−7/2250	−7/900	−7/1500
	pf			−12/875	−6/175	−18/875
	ff	48/1715	48/1715	−192/42 875	−96/8575	−288/42 875
^1P	pp	1/10	1/10	1/50	1/20	3/100
^1S	pp	2/45	2/45	−4/225	−2/45	−2/75

Table 14. $R(LSe)$ expanded into $R^k(cpde)$ and $E^k(cdpe)$ for $cdp = pdd$ (cf the caption to table 5).

LS	e	R_p^1	E_p^1	R_p^3	E_p^3	R_f^1	E_f^1	R_f^3	E_f^3	R_h^3	E_h^3
^3G	f					1	−1	1/21	−1/21		
	h									1	−1
^3F	f					1	1	−3/7	−3/7		
^3D	p	1	−1	9/49	−9/49						
	f					7/12	−7/12	1	−1		
^3P	p	1	1	−3/7	−3/7						
^3S	p	1	−1	9/14	−9/14						
^1G	f					1	1	1/21	1/21		
	h									1	1
^1F	f					1	−1	−3/7	3/7		
^1D	p	1	1	9/49	9/49						
	f					7/12	7/12	1	1		
^1P	p	1	−1	−3/7	3/7						
^1S	p	1	1	9/14	9/14						

spin integrated experiments. At first sight the general angle dependence is very complicated when spin polarization is measured. However, most or all of the possibilities can be realized in simplified geometries with the polarizations of the sample and the light and emission direction all coplanar and the spin polarization in the same plane or perpendicular to it. Also higher-order moments such as $\langle w^3 \rangle$ and $\langle w^4 \rangle$ can be observed, which are not accessible by other techniques, except nuclear quadrupole resonance. These higher-order moments are gaining new interest as the main microscopic actors in theories for the unusual ordering phenomena in heavy-fermion systems [73].

The core polarization analysis resembles the use of sum rules in x-ray absorption

spectroscopy, in that only an overall feature of the spectrum is used, whereas the whole two-dimensional spectrum of course contains much more information, especially due to the splitting caused by core–valence interactions. Hopefully it will be possible to understand what is contained in the polarization of resonances at different peaks in absorption edges, including also the LS coupled intermediate states of shallow core levels and finally decays involving valence electrons, which seem appealing because they contain information on two- and three-electron properties.

Appendix A. Coupled tensors

In order to treat any moment of a level l containing one or more holes we define the coupled tensors

$$\underline{w}_{\zeta}^{xyz} = \sum_{\xi\eta} \underline{w}_{\xi\eta}^{xy} \begin{pmatrix} x & z & y \\ -\xi & \zeta & -\eta \end{pmatrix} (-)^{x-\xi+y-\eta} \underline{n}_{xyz}^{-1} \tag{A1}$$

where $\underline{w}^{xy}$ are the uncoupled operators with x and y the orbital and spin moments.

$$\underline{w}_{\xi\eta}^{xy} = \sum_{\underline{11}} l_1 l_{\underline{1}}^{\dagger} (-)^{l-m_1} \begin{pmatrix} l & x & l \\ -m_1 & \xi & m_1 \end{pmatrix} (-)^{s-\sigma_1} \begin{pmatrix} s & y & s \\ -\sigma_1 & \eta & \sigma_1 \end{pmatrix} n_{lx}^{-1} n_{sy}^{-1}. \tag{A2}$$

Here s is used to denote the spin momentum of $\frac{1}{2}$. Substitution of (A2) into (A1) and using the graphical representation for the $3j$-symbols gives

$$\underline{w}_{\zeta}^{xyz} = \sum_{\underline{11}} l_1 l_{\underline{1}}^{\dagger} \quad \text{[graphical diagram]} \quad n_{lx}^{-1} n_{sy}^{-1} \underline{n}_{xyz}^{-1}. \tag{A3}$$

The normalizations, which remove the square roots, are defined as

$$n_{lx} = \frac{(2l)!}{\sqrt{(2l-x)!(2l+1+x)!}} \tag{A4}$$

$$n_{abc} \equiv \begin{pmatrix} a & b & c \\ 0 & 0 & 0 \end{pmatrix} \tag{A5}$$

$$\underline{n}_{abx} = i^g \left(\frac{(g-2a)!(g-2b)!(g-2x)!}{(g+1)!} \right)^{1/2} \frac{g!!}{(g-2a)!!(g-2b)!!(g-2x)!!} \tag{A6}$$

with $g = a+b+x$. When g is even and a, b and c are integers we have $\underline{n}_{abx} = n_{abx}$, but when g is odd $n_{abx} = 0$. The $\underline{n}_{abx}$ can also be used for half integer arguments.
The tensors with low values of xyz have a simple meaning:

$$\underline{w}^{000} = \underline{w}^{00} = \sum_{\underline{11}} l_1 l_{\underline{1}}^{\dagger} \delta_{\underline{11}} = n_h \tag{A7}$$

is the number of holes,

$$\underline{w}_{\xi}^{101} = -\underline{w}_{\xi}^{10} = L_{\xi} l^{-1} \tag{A8}$$

is the orbital magnetic moment,

$$\underline{w}_{\eta}^{011} = -\underline{w}_{\eta}^{01} = S_{\eta} s^{-1} \tag{A9}$$

is the spin magnetic moment,

$$\underline{w}^{110} = -(ls)^{-1} \sum_i l_i \cdot s_i \tag{A10}$$

is the spin–orbit coupling, and

$$\underline{w}_\zeta^{211} = T_\zeta (2l + 3)/l \tag{A11}$$

is the magnetic dipole operator.

The $\underline{w}^{z0z}$ with z even describe the shape (the 2^z-pole) of the charge distribution and the $\underline{w}^{x1z}$ describe spin–orbit correlations. The moments with $x + y + z$ odd describe axial couplings between spin and orbit, such as $\underline{w}^{111} = 2l^{-1}(l \times s)$.

Similar to the operators $\underline{w}$ for holes, which contain $l_1 l_{\underline{1}}^\dagger$ in (A2), we define the operators w for electrons, which contain $l_{\underline{1}}^\dagger l_1$. The difference between the two operators is a factor of -1 except for the number operator w^{00} for which we have that the number of electrons plus the number of holes is $4l + 2$.

$$w_{\xi\eta}^{xy} + \underline{w}_{\xi\eta}^{xy} = (4l + 2)\delta_{x0}\delta_{y0}. \tag{A12}$$

The operators S, L, $l \cdot s$, Q and T in (A8)–(A11) are already electron operators.

Appendix B.

B.1. General properties of angle dependent functions

We consider here angle dependent functions U constructed from spherical harmonics coupled to a totally symmetric spherical function. This function has the form of a sum of products of normalized spherical harmonics $C_{m_1}^{l_1}(P_1)C_{m_2}^{l_2}(P_2)\ldots$ with such coefficients that the total does not change when we rotate all the unit vectors P_i. An example are the angle dependence functions for resonant photoemission in cylindrical symmetry

$$U^{zarhb}(MPP_S\varepsilon) = C_\zeta^z(M)C_\alpha^a(P)C_\gamma^h(P_S)C_\beta^b(\varepsilon)$$
$$\times \sum_{\zeta\alpha\gamma\beta} \begin{pmatrix} z & a & r \\ -\zeta & -\alpha & -\rho \end{pmatrix} \begin{pmatrix} r & h & b \\ \rho & -\gamma & -\beta \end{pmatrix}$$
$$\times n_{zar}^{-1} n_{rhb}^{-1} (-)^{z-\zeta+a-\alpha+r-\rho+h-\gamma+b-\beta}. \tag{B1}$$

Upon inversion of a single vector P with associated moment l we obtain $C_m^l(-P) = (-)^l C_m^l(P)$ and so the whole function U changes by a sign $(-)^l$.

> Rule 1. *General theorem.* A totally symmetric spherical function U of a set of vectors with associated moments is zero, if a part of these vectors is perpendicular to the plane containing all the other vectors, the sum of whose moments is odd.

This can be shown by inverting all the vectors in the plane. Each inversion of a vector with moment l gives a factor $(-)^l$. The function U will thus change sign if the sum of the inverted moments is odd. But this geometry can also be obtained by a rotation of $180°$ around the axis perpendicular to the plane and so U in this geometry must have the same value as before rotation. Thus U must be zero.

B.2. Special cases

> Rule 2. *All vectors collinear.* The sum of the moments of the vectors in the plane perpendicular to them is then zero, because there are no such vectors, and so with respect to this the geometry is allowed but we may consider the collinear vectors to lie in a plane with zero vectors perpendicular to it. Then U is zero if the sum of the moments is odd.
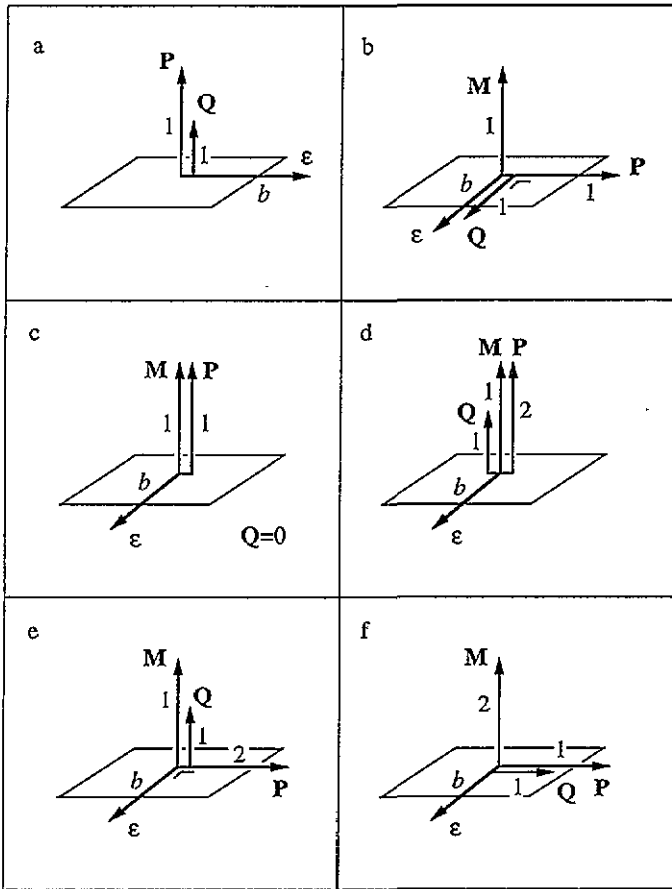
Figure B1. Geometries in which the direction of Q (the polarization vector of P_S) is fixed by the general properties of the angle dependent functions. The intensity goes as $Q \cdot P_S$. The moments z and a of the magnetization $M^{(z)}$ and the light polarization $P^{(a)}$ are given in the pictures, for the photoemission direction ε the moment b is even. (a) $M^{(0)} \to Q\|P^{(1)}$; (b) $\varepsilon\|$ or $\perp M^{(1)}$, $P^{(1)} \to Q \perp M, P$; (c) $M^{(1)}\|P^{(1)} \perp \varepsilon \to Q = 0$; (d) $M^{(1)}\|P^{(2)} \perp \varepsilon \to Q\|M$; (e) $M^{(1)} \perp P^{(2)} \perp \varepsilon \to Q\|M$; (f) $M^{(2)}$ & $P^{(1)} \to Q\|P$.

Rule 3. *All vectors coplanar.* The sum of the moments of the vectors must be even.

Rule 4. *Two sets of collinear vectors perpendicular to each other.* Both sets must be even.

Rule 5. *Three mutually perpendicular sets.* All three sets must be even or all must be odd.

B.3. Moments zero and one

Vectors with zero moment can be disregarded. Vectors with moment one are often special. If a totally symmetric function contains a vector with moment 1 it can be written as a normal inner product of two vectors

$$
\begin{array}{c}
P_a \searminus_a \quad_c d\swarmin P_d \\
P_b \swarmin^b \quad 1 \searmin P
\end{array}
= \sum_m (-)^{1-m}
\begin{array}{c}
P_a \searmin_a \quad_c d\swarmin P_d \\
P_b \swarmin^b \quad 1 \searmin_m
\end{array}
\quad
\begin{array}{c}
P \\
| \\
1 \\
|_m
\end{array}
= P \cdot Q
\tag{B2}
$$

where

$$Q_m = \quad \begin{array}{c} \mathbf{P_a} \times_a \; _c \; _d \times \mathbf{P_d} \\ \mathbf{P_b} \times_b \; _1 \diagdown_m \end{array} \tag{B3}$$

so that Q_m is a function of P_a, P_b and P_d.

We may call Q the polarization vector of P. Given the value of Q we know the whole angle dependence of the function on P, being $U = P \cdot Q$, a simple cosine dependence. Now suppose that for some choice of values for the vectors the function is zero. Then we know that the polarization vector of P must be perpendicular to P (or be zero). This information may help to fix Q completely and then we have the total dependence on P.

Special case: when we have a vector P of moment 1 and further two even sets, set_1 and set_2 of vectors perpendicular to each other the function is zero for all directions of P. This occurs e.g. in figure B1(c). Proof: consider the case where P is in the plane of set_1 and set_2. U is then zero because the total sum is odd. So Q must be perpendicular to the plane. On the other hand, if P is perpendicular to the plane, set_1 is perpendicular to the plane of P and set_2, which are together odd and U is again zero. So Q must be in the plane. This is only possible if $Q = 0$ and so the whole function is zero for any P (keeping the other vectors constant). Note that if the moment of P is not 1 but e.g. 3 then U is again zero for P either in the plane or perpendicular to it, but not necessarily in any other direction.

Figure B1 gives some examples of geometries with special consequences for the spin polarization vector that can be understood from the discussion in this appendix.

There is one important extra rule which also includes 'internal moments' such as c in (B2).

Rule 6. *Collinear reduction.* When two vectors P_a and P_b with moments a and b are coupled to c the expression is zero when P_a and P_b are parallel and $a + b + c$ is odd.

This is due to the relation

$$\begin{array}{c} \mathbf{P_a} \times \diagdown \times \mathbf{P_b} = \mathbf{P_a} \\ _a \diagdown_b \\ | \\ c \end{array} \quad = \quad \begin{array}{c} \mathbf{P_a} \\ | \\ c \end{array} \; n_{abc} \tag{B4}$$

where n_{abc} is zero for $a + b + c$ odd (cf (A5)).

References

[1] Thole B T and van der Laan G 1991 *Phys. Rev.* B **44** 12 424
[2] van der Laan G and Thole B T 1993 *Phys. Rev.* B **48** 210
[3] Thole B T and van der Laan G 1994 *Phys. Rev.* B **49** 9613
[4] Thole B T, van der Laan G and Sawatzky G A 1985 *Phys. Rev. Lett.* **55** 2086
[5] van der Laan G and Thole B T 1988 *Phys. Rev. Lett.* **60** 1977
[6] Thole B T and van der Laan G 1988 *Phys. Rev.* A **38** 1943
[7] Thole B T, Carra P, Sette F and van der Laan G 1992 *Phys. Rev. Lett.* **68** 1943
[8] Carra P, Thole B T, Altarelli M and Wang X 1993 *Phys. Rev. Lett.* **70** 694
[9] Carra P, König B T and Altarelli M 1993 *Physica* B **192** 182
[10] van der Laan G 1994 *J. Phys. Soc. Japan* **63** 2393
[11] Lenth W, Lutz F, Barth J, Kalkoffen G and Kunz C 1978 *Phys. Rev. Lett.* **41** 1185
[12] Bertel E, Stockbauer R and Madey T E 1983 *Phys. Rev.* B **27** 1939
[13] Bader S D, Zajac G and Zak J 1983 *Phys. Rev. Lett.* **50** 1211
[14] Gerken F, Barth J and Kunz C 1981 *Phys. Rev. Lett.* **47** 993
[15] Richter M, Meyer M, Pahler M, Prescher T, von Raven E, Sonntag B and Wetzel H-E 1989 *Phys. Rev.* A **40** 7007

[16] Braicovich L, Carbone C, Gunnarsson O and Olcese G L 1991 *Phys. Rev.* B **44** 13 756
[17] Muto S, Park S Y, Imada S, Yamaguchi K, Kagoshima Y and Miyahara T 1994 *J. Phys. Soc. Japan* **63** 1179
[18] Dietz R E, McRae E G, Yafet Y and Caldwell C W 1974 *Phys. Rev. Lett.* **33** 1372
[19] Davis L C and Feldkamp L A 1976 *Solid State Commun.* **19** 413; 1981 *Phys. Rev.* B **23** 6239
[20] Gunnarsson O and Li T C 1987 *Phys. Rev.* B **36** 9488
[21] Gunnarsson O 1992 *Phys. Scr.* T **41** 12
[22] Tjeng L H, Chen C T, Ghijsen J, Rudolf P and Sette F 1991 *Phys. Rev. Lett.* **67** 501
[23] Tjeng L H, Chen C T and Cheong S-W 1992 *Phys. Rev.* B **45** 8205
[24] van der Laan G, Surman M, Hoyland M A, Flipse C F J, Thole B T, Seino Y, Ogasawara H and Kotani A 1992 *Phys. Rev.* B **46** 9336
[25] van der Laan G, Thole B T, Ogasawara H, Seino Y and Kotani A 1992 *Phys. Rev.* B **46** 7221
[26] Qvarford M, van Acker J F, Anderson J N, Nyholm R, Lindau I, Chiaia G, Lundgren E, Söderholm S, Karlsson U O, Foldström S A and Leonyuk L 1995 *Phys. Rev.* B **51** 410
[27] van der Laan G 1994 *Int. J. Mod. Phys.* B **8** 641
[28] Tanaka A and Jo T 1992 *J. Phys. Soc. Japan* **61** 3837
[29] Tanaka A and Jo T 1992 *J. Phys. Soc. Japan* **61** 2669
[30] Allen J W 1991 *Synchrotron Radiation Research: Advances in Surface Science and Low Dimensional Science* ed R F Bachrach (New York: Plenum) ch 8
[31] Laubschat C, Weschke E, Kalkowski G and Kaindl G 1990 *Phys. Scr.* **41** 124
[32] Kaindl G, Navas E, Arenholz E, Baumgarten L and Starke K 1995 *Core Level Spectroscopies for Magnetic Phenomena: Theory and Experiment (NATO ASI Series)* ed P Bagus, F Parmigiani and G Pacchioni (New York: Plenum) p 131
[33] Park J-H, Tjeng L H, Allen J W, Claessen R, Chen C T, Metcalf P and Harrison H R, unpublished
[34] Tanaka A and Jo T 1994 *J. Phys. Soc. Japan* **63** 2788
[35] Tjeng L H, Chen C T, Rudolf P, Meigs G, van der Laan G and Thole B T 1993 *Phys. Rev.* B **48** 13 378
[36] Nicklin C L, Binns C, Mozley S, Norris C, Alleno E, Bartés-Labrousse M-G and van der Laan G 1995 *Phys. Rev.* B **52** 4815
[37] Thole B T, Dürr H A and van der Laan G 1995 *Phys. Rev. Lett.* **74** 2371
[38] Flügge S, Mehlhorn W and Schmidt V 1972 *Phys. Rev. Lett.* **29** 7
[39] Cleff B and Mehlhorn W 1974 *J. Phys. B: At. Mol. Phys.* **7** 593
[40] Cleff B and Mehlhorn W 1974 *J. Phys. B: At. Mol. Phys.* **7** 605
[41] McFarlane S C 1972 *J. Phys. B: At. Mol. Phys.* **5** 1906
[42] Kabachnik N M and Sazhina I P 1976 *J. Phys. B: At. Mol. Phys.* **9** 1681
[43] Berezhko E G, Kabachnik N M and Rostovsky V S 1977 *J. Phys. B: At. Mol. Phys.* **11** 1749
[44] Klar H 1980 *J. Phys. B: At. Mol. Phys.* **13** 4741
[45] Barschat K 1981 *Phys. Rep.* **180** 1
[46] Kabachnik N M 1981 *J. Phys. B: At. Mol. Phys.* **14** L337
[47] Blum K, Lohmann B and Taute E 1986 *J. Phys. B: At. Mol. Phys.* **19** 3815
[48] Kabachnik N M and Lee O V 1989 *J. Phys. B: At. Mol. Opt. Phys.* **22** 2705
[49] Lohmann B 1990 *J. Phys. B: At. Mol. Opt. Phys.* **23** 3147
[50] Lohmann B 1991 *J. Phys. B: At. Mol. Opt. Phys.* **24** 861
[51] Kabachnik N M 1992 *J. Phys. B: At. Mol. Opt. Phys.* **25** L389
[52] Stoppmanns P, Schmiedeskamp B, Vogt B, Müller N and Heinzmann U 1992 *Phys. Scr.* **T41** 190
[53] Berakdar J, Klar H, Huetz A and Selles P 1993 *J. Phys. B: At. Mol. Opt. Phys.* **26** 1463
[54] Lohmann B, Hergenhahn U and Kabachnik N M 1993 *J. Phys. B: At. Mol. Opt. Phys.* **26** 3327
[55] Lohmann B and Larkins F P 1994 *J. Phys. B: At. Mol. Opt. Phys.* **27** L143
[56] Cowan R D 1981 *The Theory of Atomic Structure and Spectra* (Berkeley, CA: University of California Press)
[57] Clauberg R, Gudat W, Kisker E, Kuhlman E and Rothberg G M 1981 *Phys. Rev. Lett.* **47** 1314
[58] Davis L C 1985 *J. Appl. Phys.* **59** R25
[59] Sakurai J J 1967 *Advanced Quantum Mechanics* (New York: Addison-Wesley) ch 2.6
[60] Aberg J and Howat G 1982 *Handbuch der Physik* vol 31, ed W Mehlhorn (Berlin: Springer) p 469
[61] Almbladh C-O and Hedin L 1983 *Handbook on Synchrotron Radiation* vol 1b, ed E-E Koch (Amsterdam: North-Holland) ch 8
[62] Rehr J J and Alberts R C 1990 *Phys. Rev.* B **41** 8139
[63] Fadley C S 1992 *Synchrotron Radiation Research* vol 1, ed R F Bachrach (New York: Plenum) p 421
[64] Idzerda Y U and Ramaker D E 1992 *Phys. Rev. Lett.* **69** 1943
[65] Ramaker D E, Yang H and Idzerda Y U 1994 *J. Electron Spectrosc. Relat. Phenom.* **68** 63
[66] Zare R N 1988 *Angular Momentum* (New York: Wiley)

[67] Yutsis A P, Levinson I B and Vanagas V V 1962 *Mathematical Apparatus of the Theory of Angular Momentum* (Jerusalem: Israel Program for Scientific Translation)

[68] Brink D M and Satchler G R 1962 *Angular Momentum* (Oxford: Clarendon) ch 7

[69] Varshalovich D A, Moskalev A N and Khersonskii V K 1988 *Quantum Theory of Angular Momentum* (Singapore: World Scientific) p 438

[70] Biedenharn L C and Louck J D 1981 *Angular Momentum in Quantum Physics (Encyclopedia of Mathematics 8)* (Reading, MA: Addison-Wesley) section 8c

[71] van der Laan G 1995 *Phys. Rev.* B **51** 240

[72] Goldberg S M, Fadley C S and Kono S 1981 *J. Electron Spectrosc. Relat. Phenom.* **21** 285

[73] Cox D L 1987 *Phys. Rev. Lett.* **59** 1240